

Sedimentary Cyclicality in CRP Drillcore, Victoria Land Basin, Antarctica

T.R. NAISH^{1*}, P.J. BARRETT², G.B. DUNBAR^{3§}, K.J. WOOLF^{3†}, A.G. DUNN⁴, S.A. HENRYS¹,
M. CLAPS^{5‡}, R.D. POWELL⁶ & C.R. FIELDING⁷

¹Institute of Geological and Nuclear Sciences, P.O. Box 30368, Lower Hutt - New Zealand

²Antarctic Research Centre, Victoria University of Wellington, PO Box 600 - New Zealand

³School of Earth Sciences, James Cook University, Townsville, Queensland 4611 - Australia

⁴National Institute of Water and Atmospheric Research, P.O. Box 14901, Wellington - New Zealand

⁵Instituto di Scienze del Mare, Università degli Studi di Ancona, Via Breccie Bianche, Ancona - Italy

⁶Department of Geology, Northern Illinois University, DeKalb, IL 60115 - USA

⁷Department of Earth Sciences, University of Queensland, Brisbane, Queensland 4072 - Australia

[§]Present address: Antarctic Research Centre, Victoria University of Wellington, PO Box 600 - New Zealand

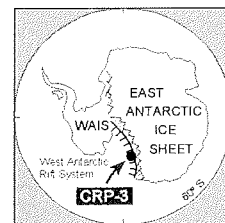
[†]Deceased

[‡]Present address: Agip Kazakhstan North Caspian Operating Company, N.V.Raamweg 26, 2596 HL, The Hague - The Netherlands

Received 12 March 2001; accepted in revised form 20 August 2001

Abstract - The upper 1200 m of pre-Pliocene sediment recovered by Cape Roberts Project (CRP) drilling off the Victoria Land coast of Antarctica between 1997-1999 has been subdivided into 54 unconformity-bound stratigraphic sequences, spanning the period c. 32 to 17 Ma. The sequences are recognised on the basis of the cyclical vertical stacking of their constituent lithofacies, which are enclosed by erosion surfaces produced during the grounding of the advancing ice margin onto the sea floor. Each sequence represents deposition in a range of offshore shelf to coastal glacial marine sedimentary environments during oscillations in the ice margin across the Western Ross Sea shelf, and coeval fluctuations in water depth.

This paper applies spectral analysis techniques to depth- and time-series of sediment grain size (500 samples) for intervals of the core with adequate chronological data. Time series analysis of 0.5-1.0m-spaced grain size data spanning sequences 9-11 (CRP-2/2A) and sequences 1-7 (CRP-3) suggests that the length of individual sequences correspond to Milankovitch frequencies, probably 41 k.y., but possibly as low as 100 k.y. Higher frequency periodic components at 23 k.y. (orbital precession) and 15-10 k.y. (sub-orbital) are recognised at the intrasequence-scale, and may represent climatic cycles akin to the ice rafting episodes described in the North Atlantic Ocean during the Quaternary. The cyclicality recorded by glacial marine sequences in CRP core provides direct evidence from the periphery of Antarctica for orbital oscillations in the size of the Oligocene-Early Miocene East Antarctic Ice Sheet.



INTRODUCTION

Long sedimentary records containing only a limited number of rock types will nearly always display depositional cyclicality, regardless of the processes of deposition (summarised in Schwarzacher, 1999). In many cases such sedimentary cyclicality is strongly ordered, and comprises repetitive cycles of facies or lithologies. An oscillating forcing mechanism is usually inferred to have generated this type of cyclicality. The astronomical variation in Earth's orbit is the most significant oscillating system which has been shown to force climate and sedimentary cyclicality. It produces the periodic, so-called "Milankovitch" cycles. In its traditional form Milankovitch theory states that long term, orbitally-controlled changes in high-latitude summer insolation cause predictable waxing and waning of continental ice-sheets, and therefore, periodic variations in global climate (e.g.

Milankovitch, 1995). The causal link between astronomical-forcing of climate and sedimentation has been well established since the seminal work of Hays et al. (1976) on deep-sea benthic $\delta^{18}\text{O}$ records. Milankovitch cycles are now routinely recognised in deep-ocean sediment cores, where sedimentation rates are more or less constant. Spectral analysis of deep ocean proxy climate records (e.g. magnetic susceptibility, grey scale, gamma ray attenuation, $\delta^{18}\text{O}$) usually reveals periodic orbital components (precession, obliquity and eccentricity) with amplitudes well above the background noise levels (e.g. Zachos et al., 1997).

However, in continental margin settings a variety of non-cyclic sedimentary processes occur, such as current erosion, sediment gravity flows, storm events, delta-lobe switching and tectonism, which cause the resulting record to be complex and to contain both random and periodic components. The 1500m-thick

*Corresponding author (t.naish@gns.cri.nz)

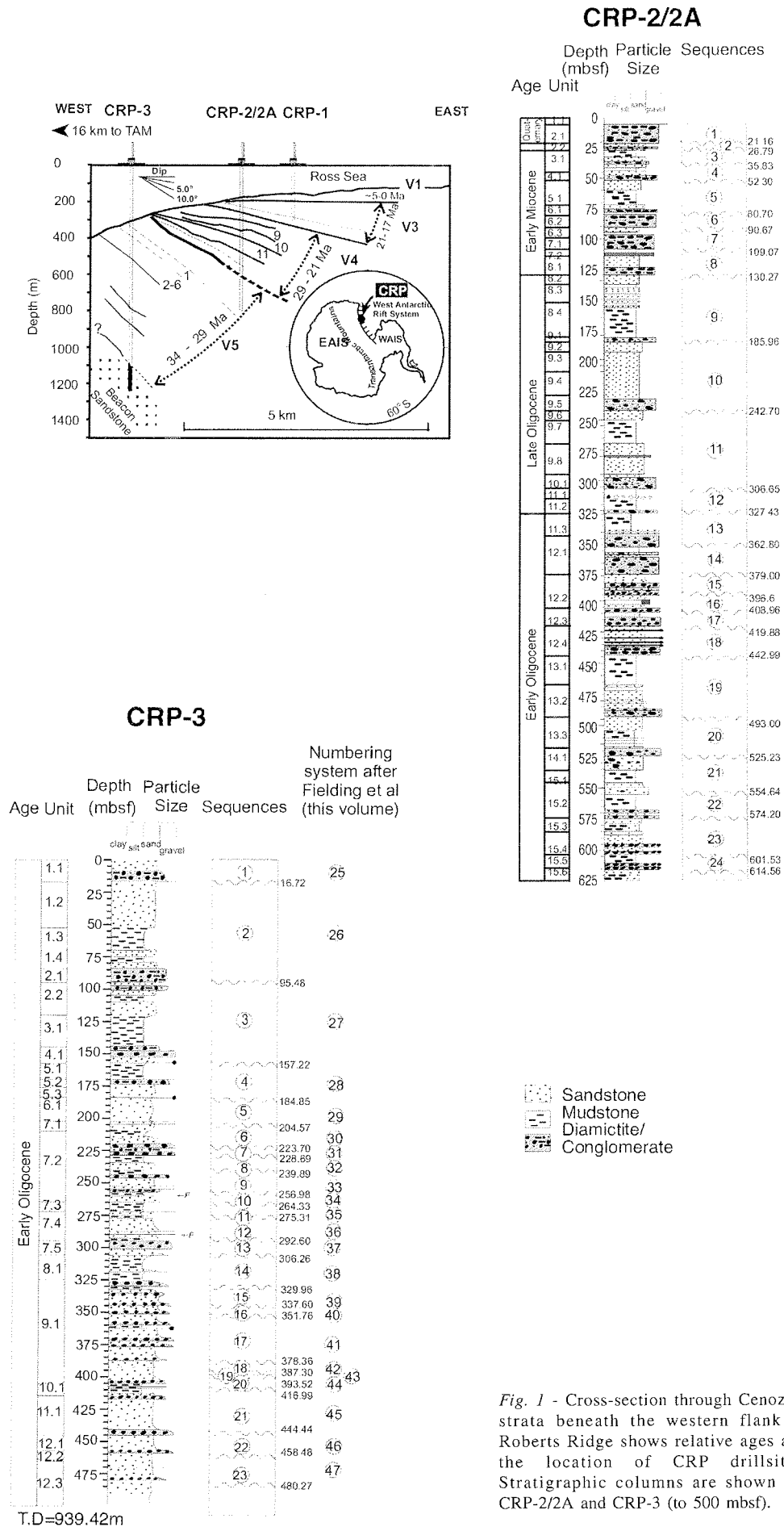


Fig. 1 - Cross-section through Cenozoic strata beneath the western flank of Roberts Ridge shows relative ages and the location of CRP drillsites. Stratigraphic columns are shown for CRP-2/2A and CRP-3 (to 500 mbsf).

sediment record cored by the multinational Cape Roberts Project (CRP) off the Victoria Land coast of Antarctica (Fig. 1; Cape Roberts Science Team, 1999; 2000), displays a complex cyclostratigraphic architecture. A total of 54 unconformity-bounded glaci-marine sequences have been identified in core from the three Cape Roberts drillholes (Cape Roberts Science Team, 2000, 2001), and the facies architecture of those from CRP-2/2A (24) and CRP-3 (23) has been analysed by Fielding, Naish and Woolfe (this volume). The thickest of these sequences (*e.g.* >50m) have also been identified in seismic reflection profiles (Fig. 2; Fielding et al., this volume; Henrys et al., 2000). Each cycle contains a repetitive vertical succession of facies which are interpreted to represent recurrent cycles of advance and retreat of grounded ice across the Ross Sea continental shelf. It has also been suggested that changes in relative sea level of up to 50 m magnitude may have occurred in concert with local ice margin movements.

Milankovitch periodicities have been reported for $\delta^{18}\text{O}$ records from deep-sea sediment cores across the Oligocene-Miocene boundary (Shackleton et al., 2000), and various interpretations have been drawn from the data regarding the nature and behaviour of Antarctica's ice sheets (Zachos et al., 1997; Paul et al., 2000). However, until the drilling of the CRP-2/2A drillhole in western Ross Sea, no ice-marginal record afforded the possibility of identifying Milankovitch-scale palaeoenvironmental changes from strata from the periphery of Antarctica. This was because of the lack of suitable cores and the lack of the chronological data needed to resolve such patterns. Thus, inferences about the Antarctic ice sheets made from low-latitude sediment cores have remained largely unsubstantiated. An integrated chrono- (Wilson et al., 2000) and sequence-stratigraphic analysis (Fielding et al., 2000) allowed Naish et al. (2001) to identify 3 sequences in core from CRP-2/2A (sequences 9, 10 & 11) spanning the Oligocene-Miocene boundary whose durations are consistent with deposition induced by known orbital rhythms in contemporary insolation (Laskar et al., 1993; Shackleton et al., 1999).

This paper attempts to evaluate further the nature and periodicity of sedimentary cyclicality over the portions of the CRP glaci-marine record for which there is adequate chronological data, by undertaking spectral analysis of grainsize depth and time series. The recognition of periodic from non-periodic cycles in the CRP core is of critical importance if the role of orbital forcing on (1) shallow-marine sedimentation in the western Ross Sea, and (2) the adjacent East Antarctic Ice Sheet is to be properly understood. The grainsize data are analysed at two different spatial and temporal resolutions:

Sequence-scale - 0.5-1.0m-spaced percentage sand depth and time series data spanning sequences 9-11 (128 to 306.65 mbsf; CRP-2/2A) and sequences 1-7 (13.0 to 230.0 mbsf; CRP-3).

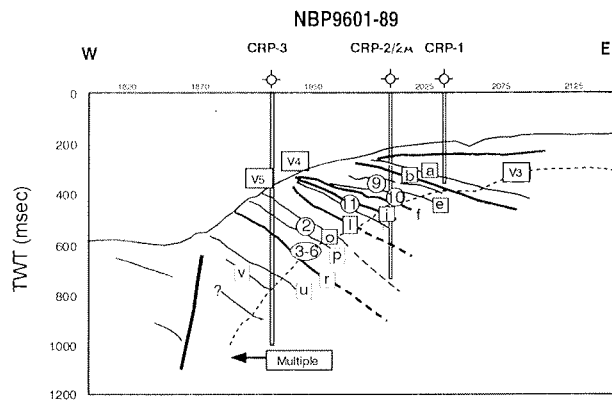


Fig. 2 - Seismic reflection profile NBP9601-89 showing geometry of Cenozoic strata beneath the western flank of Roberts ridge and the location of CRP drillsites (after Henrys et al., this volume). Prominent seismic reflectors identified by Henrys et al. are labelled (a-v). Correlation of some of the reflectors with sequences recognised in CRP-2/2A and CRP-3 is after Fielding et al. (this volume). CRP-2/2A sequences 9, 10 and 11 and CRP-3 sequences 2-6 are shown on the seismic line.

Intrasequence-scale - 0.5-1.0m-spaced percentage sand depth and time series data spanning two characteristic vertically-stacked facies successions; sequence 11 (CRP-2/2A) and sequence 2 (CRP-3) 267.25m), (D) Facies 5, sequence 12 (319.32-320.32m), (E) Facies 1, sequence 20 (504.60-505.34m).

METHODS

GRAIN SIZE DATA

One hundred and seventy samples (each *c.* 1 cc) were collected at *c.* 0.5m-1.0m-spaced intervals between 128.72 and 306.65m in CRP-2/2A (Appendix 1), and 334 samples (*c.* 1 cc) were collected at *c.* 0.5m-spaced intervals between 13.0 and 230.0m from CRP-3 (Appendix 2) to investigate sedimentary cyclicality at the sequence- and intrasequence-scale. Analyses were carried out at the Sedimentology Laboratory at James Cook University using a Malvern Instruments Mastersizer-X laser particle size analyser (*e.g.* Woolfe et al., 1999) fitted with a 300 mm focal length lens. Sample weights ranging from ~0.3 g for mudstone to ~3 g for sandstone were used in order to obtain an optimal laser "obscuration" value of ~20%. Samples were prepared for analysis using a combination of physical and mechanical disaggregation methods. Initially, samples were mechanically disaggregated by crushing, or gentle grinding with wooden blocks until rendering aggregates >~2 mm in size. In order to remove organic matter and further aid disaggregation, samples were subsequently immersed in 10% H_2O_2 solution and placed in a heated (85°C) ultrasonic water bath for approximately one hour, or until inspection under binocular microscope showed

complete disaggregation to primary depositional grain sizes. Following this, samples were then centrifuged at 3000 rpm for 15 minutes and the supernatant liquid decanted. Any remaining carbonate was treated with 10% HCl until effervescence ceased. All samples were then re-washed in water and centrifuged. Once the supernatant liquid had been removed the solids were resuspended in 50 ml of water and sonicated for a further 10 minutes and wet sieved at 1000 μm to remove coarse sediment immediately prior to analysis. Experience has shown that material finer than the minimum size of the lens can create artefacts in the size distribution (see Fielding, Dunbar & Bryce, this volume). For the 300 μm lens this results in a "false" mode at 2.2 μm . Although this mode does not accurately reflect the size frequency distribution less than $\sim 5 \mu\text{m}$, the area under the mode is approximately proportional to the amount of sediment finer than $\sim 5 \mu\text{m}$.

SPECTRAL ANALYSIS

Spectral analysis is used to evaluate the observed depositional cyclicality within the CRP-2/2A and CRP-3 percent-sand size data series. The programme used in this paper is called SPECTRUM (Shulz & Stattegger, 1998) and was developed specifically to overcome the problems encountered with unevenly spaced stratigraphic data sets. SPECTRUM is based on the Lomb-Scargle Fourier transform (LFST; Lomb, 1976; Scargle, 1982, 1989) for unevenly spaced time series in combination with a Welch-Overlapped-Segment-Averaging procedure (WOSA; Welch, 1967; cf. Percival & Walden, 1993, p. 289) for consistent spectral estimates.

In all cases, harmonic analysis is applied to both depth and time series from the cores in order to detect periodic signal components (e.g. Milankovitch and sub-Milankovitch frequencies) in the presence of noise (non-periodic sedimentary or random noise). As continental margin palaeoclimatic time series are most frequently embedded in a red noise background, which usually results from non-periodic depositional processes, SPECTRUM utilises Siegel's (1980) test for the identification of up to three periodic components within a normalised periodogram of depth/time series data. In some cases a smoothing procedure is used that essentially broadens the bandwidth of complex periodic components.

A significant problem encountered with undertaking spectral analysis on unevenly-spaced data from continental margin sedimentary records is that sedimentation rates, which are facies-dependent, may vary significantly through the time series. Thus, when calibrating depth data to an age model there are 2 possible approaches: (1) one can make certain assumptions about sedimentation rate, or (2) one interpolates age data in a linear fashion between calibration points independently of sedimentation rate.

Experiments conducted on Quaternary, orbitally-influenced, shallow-marine sedimentary cycles, Wanganui Basin, New Zealand (Naish et al., 1998; Naish et al., unpublished data), indicate that incorrect estimation of sedimentation rate results in significantly more reddening of the frequency spectrum than linear interpolation of age data between calibration points. This is particularly true in high sedimentation rate settings ($>1\text{m/k.y.}$), such as the Victoria Land Basin. Thus, time series are only constructed for intervals of the CRP core where chronologies are relatively robust, and circular arguments involving estimation of sedimentation rate to assign time to the sedimentary succession are not used.

An additional problem is the length of time series being analysed by spectral techniques, particularly at the intrasequence scale. While we acknowledge that the CRP data series are probably too short to yield reliable periodic components at the low-frequency end of the spectrum, powerful periodic components do occur well above background noise levels, and these correspond to Milankovitch durations and thicknesses of individual sequences. Thus, although statistically-speaking these peaks may lack rigour, they do correspond to observed grainsize cyclicality at the sequence-scale.

LITHOLOGICAL & GRAINSIZE SIGNATURE

Variations in sand content upsection within CRP-2/2A and CRP3 sequences (Figs. 4 & 5) show close correspondence to vertical changes in lithofacies with time (Figs. 6 & 7). The lower parts of sequences display a broad fining upwards trend from pebbly sandstone (facies 5), conglomerate (facies 9 & 10) and diamictite (facies 6 & 7) to poorly sorted muddy sandstone (facies 3) and interstratified mudstone and sandstone (facies 2 & sometimes facies 8) with decreasing numbers of outsized clasts. Sand content progressively decreases upwards from 100-60% to $<10\%$. The transition to fine-grained facies is abruptly gradational, in most cases occurring over a 1m interval. The mid-cycle interval is characterised by sparsely fossiliferous, bioturbated mudstone (facies 1) ($<10-30\%$). Upper parts of sequences display an overall coarsening upwards regressive lithofacies succession from mudstone (facies 1) to sandy mudstone (facies 2 & 3) to well sorted sandstone (facies 4) with increasing amounts of coarser-grained sand and gravel, and tractional sedimentary structures. Sand content increases upward from $<30\%$ up to 100%. Where coarsening upward regressive successions are not truncated at the superjacent sequence boundary, the transition from fine-grained to coarse-grained sediments may be abrupt and in some cases marked by minor erosional relief.

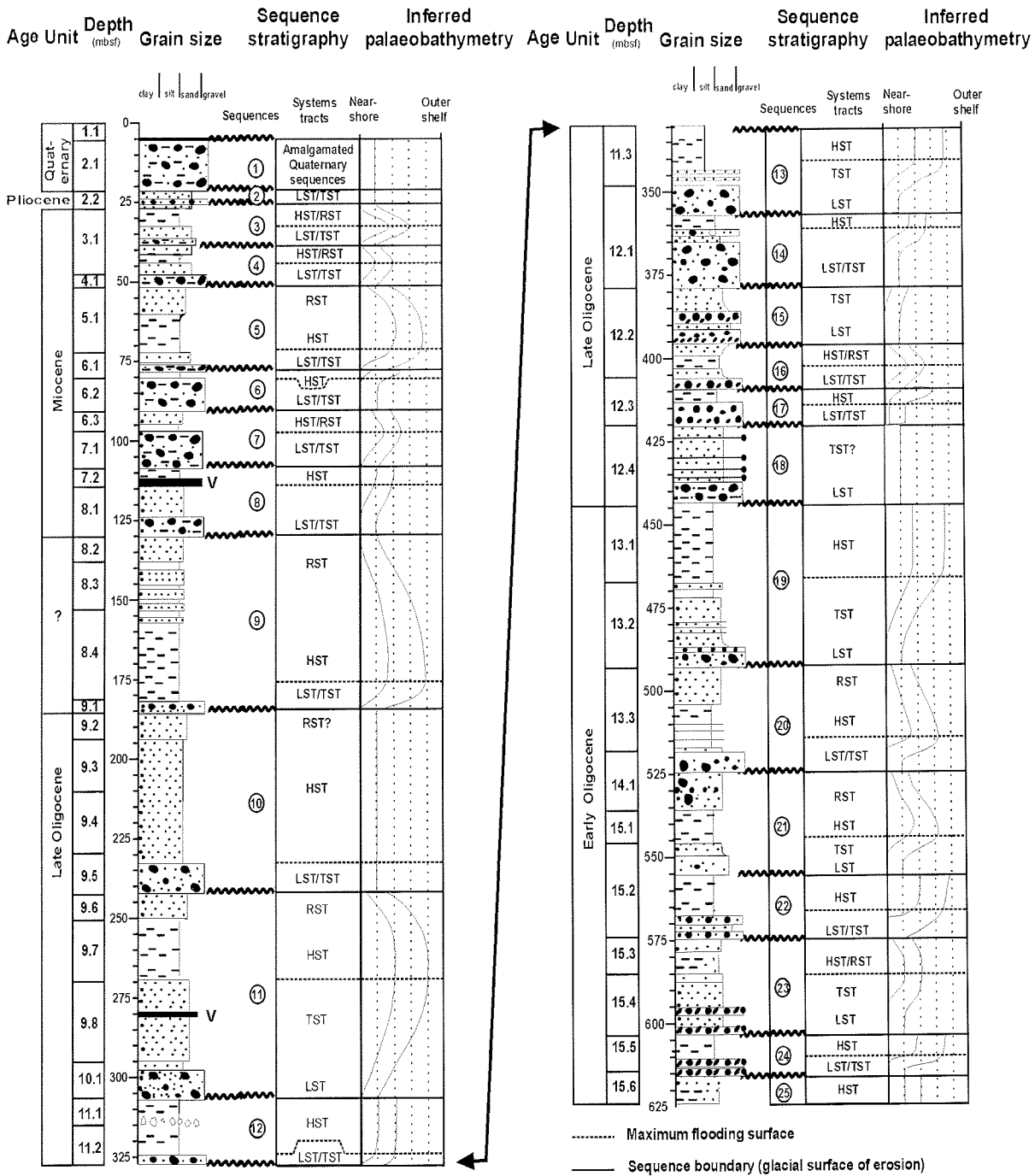


Fig. 3 - Sequence stratigraphical interpretation of CRP-2/2A lithostratigraphy and inferred palaeobathymetric changes within sequences (after Fielding et al., 2000; Cape Roberts Science Team, 1999).

SEQUENCE STRATIGRAPHIC INTERPRETATION

Ten to 90m-thick, unconformity bound sedimentary cycles, termed sequences¹ contain a repetitive vertical succession of facies, which are interpreted to represent recurrent cycles of advance

and retreat of grounded ice across the Ross Sea continental shelf, in concert with cyclical changes in water depth (Fielding et al., 2000; this volume). The CRP-2/2A and CRP-3 sequences are illustrated in figures 3, 4 and 5, and are considered to have been deposited seaward of the contemporary coast as part of a laterally extensive seaward-thickening nearshore

¹ The term "sequence" has a specific usage that was developed from studies of non-glaciated continental margins, where it is applied to unconformity-bound packages of strata that are inferred to have accumulated during a cycle of relative sea-level change (e.g. Vail et al., 1987). We have extended the use of the term "sequence" to a glacial marine sedimentary cycle, bounded by sharp erosion surfaces produced by an advance-retreat-readvance cycle of an ice margin across the shelf, in concert with an oscillation of relative water depth (Fielding et al., 2000).

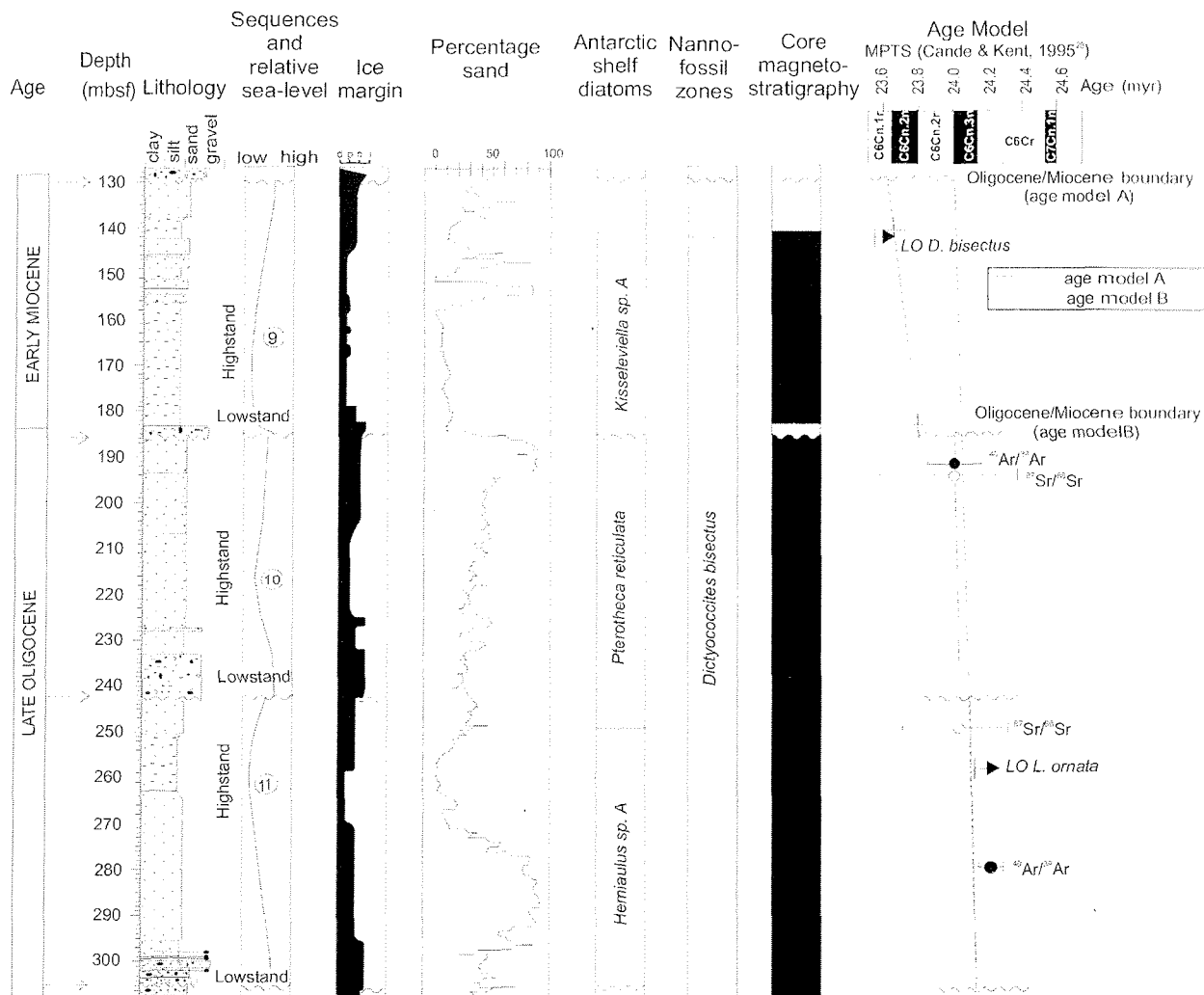


Fig. 4 - Sequence stratigraphical interpretation (Fielding et al., 2000) of CRP-2/2A lithostratigraphy, ice margin proximity (Cape Roberts Science Team, 1999), percentage sand, inferred palaeobathymetric changes inferred from facies analysis (Fielding et al., 2000; Powell et al., 2000), and age models (Wilson et al., 2000; Naish et al., 2001) for sequences 9, 10 and 11 (128.72 to 305.65). Key for the interpretation of ice margin proximity: "n" = non-glacial (marine), "d" = distal glacimarine, "p" = proximal glacimarine, "i" = ice contact

sediment wedge. We hypothesise that during periods of glacial advance the interior East Antarctic Ice Sheet (EAIS), fed through the Transantarctic Mountains as a series of outlet glaciers which fed to a laterally extensive marine ice terminus which was grounded on the Ross Sea continental shelf beyond the CRP drill sites (Naish et al., 2001). Thus cycles of ice margin advance and retreat across the shelf are viewed as cycles of expansion and contraction of the EAIS.

We interpret each sequence (Figs. 4 & 5) in terms of a sequence stratigraphical model (Figs. 6 & 7) adapted to glacimarine sedimentary successions (Fielding et al., 2000). Each begins with a sharp planar to sub-horizontal eroded surface, *the glacial surface of erosion*, which records local ice margin, and advance across the sea floor during glacio-eustatic sea-level fall. The lithofacies which overlie the basal unconformity represent deposition in a range of offshore shelf to shallow-marine coastal

sedimentary environments during the relative rise, highstand, and fall of sea level. In contrast to non-glaciated, low latitude margins, CRP core contains direct sedimentary evidence (glacigenic features) for ice volume changes together with evidence supporting bathymetric fluctuations.

The vertical succession in CRP sequences is interpreted as follows: (1) erosion and minor deposition during ice margin advances followed by a fining upwards interval deposited during ice margin retreat and bathymetric deepening (lowstand/transgressive systems tract); (2) an interval of relatively ice-free open marine pelagic sediment (highstand systems tract); and (3) a coarsening-upwards regressive succession representing re-advance of the ice margin into a shallow marine setting in association with bathymetric shoaling (regressive systems tract). The sedimentary features used to arrive at these interpretations are presented in more detail by Fielding et al (2000; this volume) and Powell et al.

(2000, this volume). However, it is important to note that the sedimentological and faunal palaeobathymetric indicators which occur suggest that intra-sequence water depth changes of up to ~50 m occurred in concert with ice margin advance and retreat cycles (Cape Roberts Science Team, 1999; Fielding et al., 2000).

GLACIAL AND SEA LEVEL SIGNATURE

The stratigraphic variations in grainsize and lithofacies which occur in the Cape Roberts drillcore primarily reflect oscillations in depositional energy, themselves controlled by the combination of changes

in water depth and glacial proximity. Data supporting such an interpretation are presented elsewhere in this volume (Fielding et al., this volume; Barrett, this volume). Such inferences are consistent with established depositional models of temperate and polythermal glaciers entering into the sea (Powell et al., 1981), and models of shallow marine sedimentation during orbitally-driven cyclical changes in relative sea level (Abbott & Carter, 1994; Naish & Kamp, 1997).

Grainsize histograms for c. 5m-spaced intervals up-core are shown for sequence 11, CRP-2/2A (Fig. 6) and sequence 2, CRP-3 (Fig. 7). The grainsize variations within a sequence, described above, are clearly supported by systematic

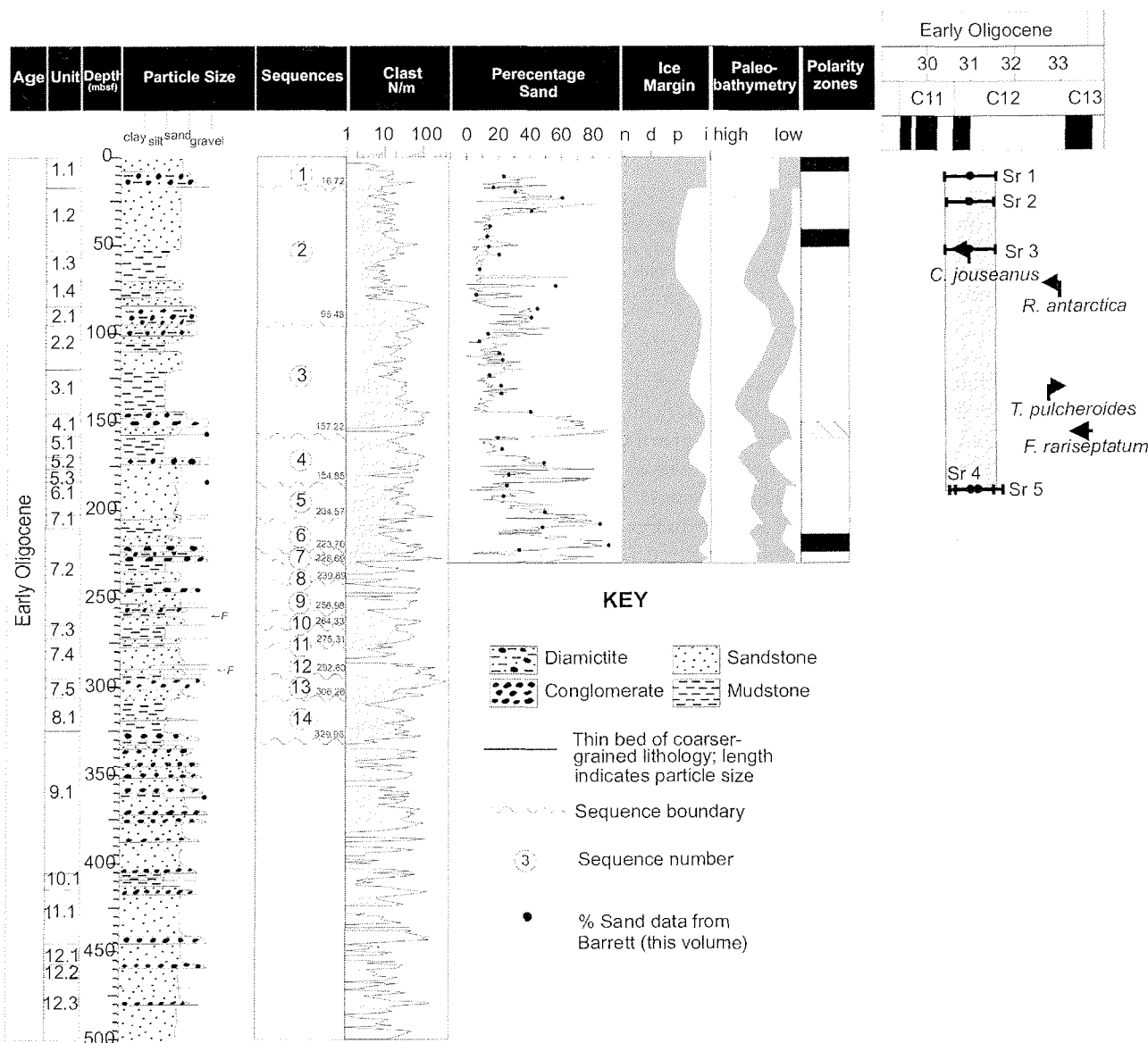


Fig. 5 - Sequence stratigraphical interpretation of CRP-3 lithostratigraphy from 0 to 329.26 mbsf (after Fielding et al., this volume; Cape Roberts Science Team, 2000). Also shown is the down core variation in clast abundance (>2mm; after Sandroni & Talarico., this volume), percentage sand, ice margin proximity (Cape Roberts Science Volume, 2000), inferred palaeobathymetry (Cape Roberts Science Volume, 2000), and the age model for sequences 1 to 5 (Hannah et al., this volume). Key for the interpretation of ice margin proximity: "n"= non-glacial (marine), "d"= distal glacial, "p"= proximal glacial, "i"=ice contact

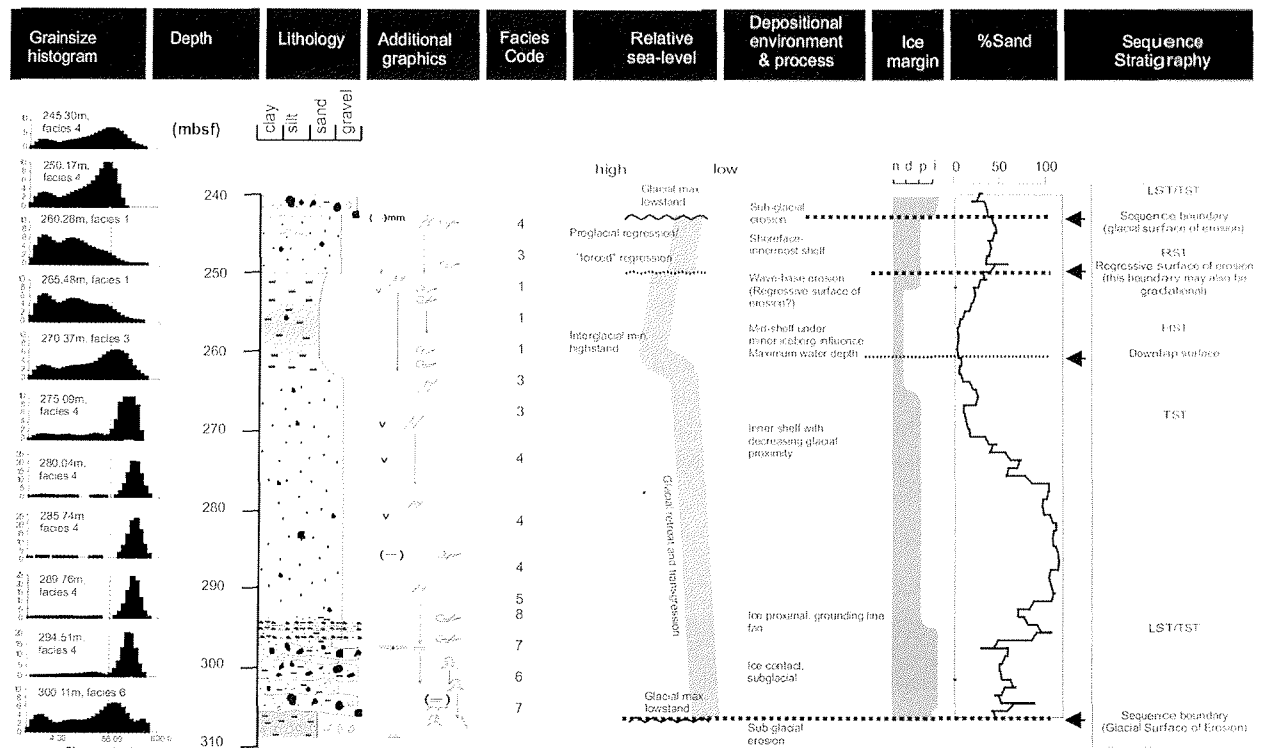


Fig. 6 - High-resolution grainsize analysis of CRP-2/2A, sequence 11. Variations in grainsize distribution are shown for representative samples up-sequence. Note that histograms and sand abundance are consistent with lithological description of the core and facies interpretations (Feilding et al., 2000; Powell et al., this volume). Sequence stratigraphy, depositional environments, glacial proximity and inferred palaeobathymetric changes are interpreted from facies and lithological analysis (also see Barrett et al., this volume). "n"=non-glacial, "d"=ice distal, "p"=ice proximal and "i"= ice contact.

stratigraphic change in the position of the mode of the distribution. Both sequences are characterised by bimodal and in some cases trimodal grainsize histograms. The exception is an interval of sandstone within the lower part of sequence 11, between c. 265 to 295m, which is moderately-well sorted (facies 4), unimodal, but skewed with a coarse-tail. Barrett (this volume) interprets this style of grainsize distribution as representing the admixture of an outsized ice rafted component with a well-sorted, shallow-marine sandstone which was deposited above wave-base. However, the generally polymodal nature of the grainsize distribution is consistent with mixing of sediments from different source areas, most likely by a range of glacial-marine processes (Powell et al., this volume) superimposed on a wave-graded, open coastline and inner shelf (Barrett, this volume).

CYCLE DURATION AND PERIODICITY AT THE SEQUENCE SCALE

CRP-2/2A

Age Model

The age model used to construct time series for sequences 9, 10 and 11 is based on a combination of single crystal $^{40}\text{Ar}/^{39}\text{Ar}$ ages on volcanic material, microfossil biostratigraphy, $^{87}\text{Sr}/^{86}\text{Sr}$ analyses of molluscs, and correlation of a magnetic polarity

zonation to the magnetic polarity time scale (Wilson et al., 2000; Naish et al., 2001). Two possible constructions for the age/depth curve illustrated in figure 5 are allowed by the chronological data for sequences 9-11 (Wilson et al., 2000). The two models are the consequence of differing interpretations of a 4m-thick magnetically reversed interval of diamictite and sandstone at the base of sequence 9. The first age model (age model A) described below correlates the N-R-N-R up-core magnetostratigraphy data with the Polarity Chrons C6Cn.3n, C6Cn.2r, C6Cn.2n and C6Cn.1, respectively. This age model correlates the thin reversed polarity interval at the base of Sequence 9 with C6Cn.2r. The second age model (age model B) described below interprets the thin reversed polarity interval at the base of Sequence 9 as a short duration polarity excursion and correlates the interval of core comprising sequences 9-11 with C6Cn.3n. It has been argued that such excursions, if present, are more likely to be recorded in high sedimentation rate sedimentary settings, and indeed other short polarity excursions are recognised in Chron C12r which is correlated with the upper part of CRP-3 (Florindo et al., this volume). Age model B is consistent with all of the chronostratigraphic data, but requires the recognition in CRP-2/2A of a previously unreported short duration polarity reversal within C6Cn.3n.

Age model A provides the least constraint of the two options, as it restricts the duration of the 3 cycles

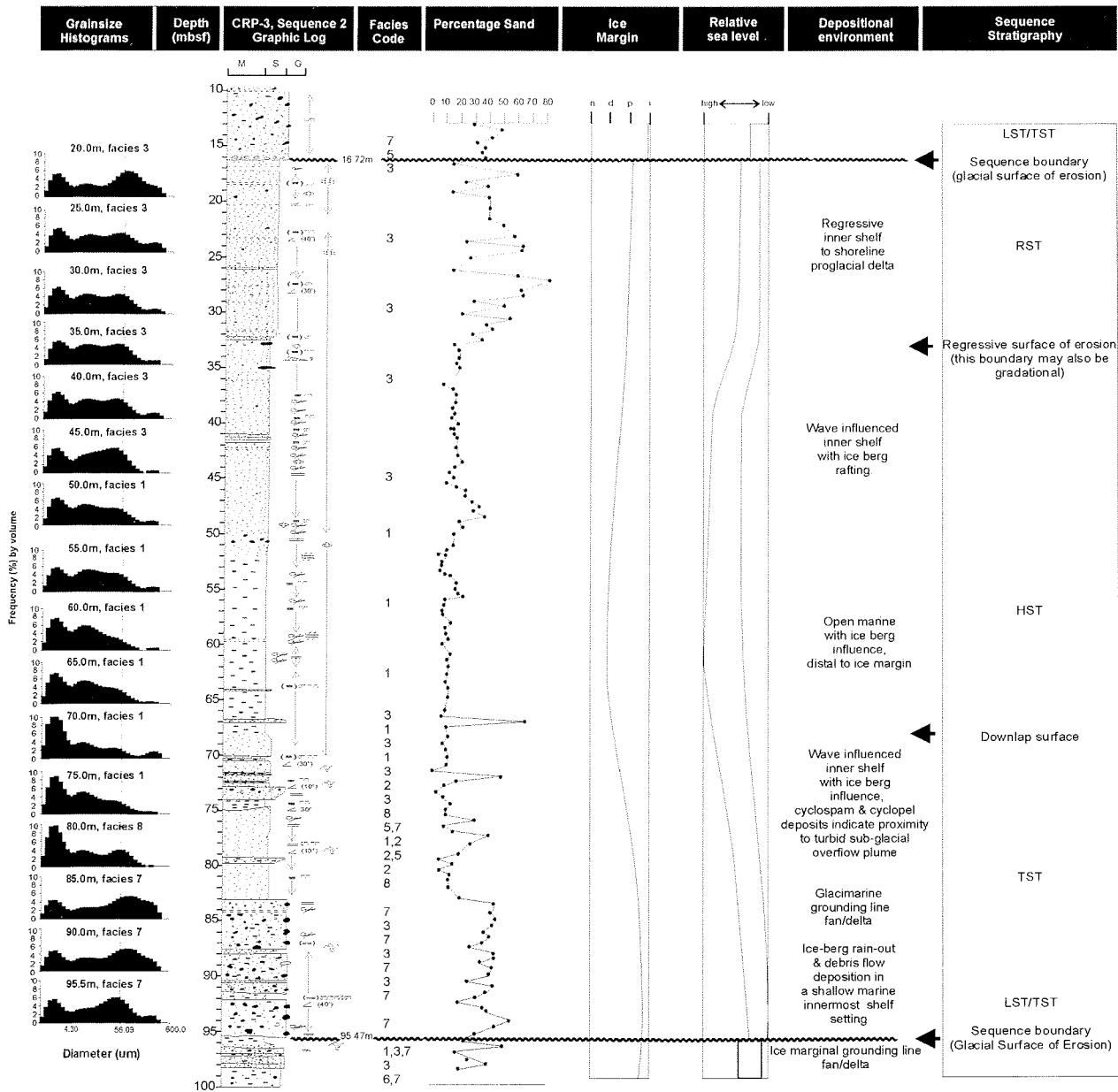


Fig. 7 - High-resolution grainsize analysis of CRP-3, sequence 2 (16.72m to 95.47m). Variations in grainsize distribution are shown for representative samples up-sequence. Note that histograms and sand abundance are consistent with lithological description of the core and facies interpretations (Powell et al., this volume). Sequence stratigraphy, depositional environments, glacial proximity and inferred palaeobathymetric changes are interpreted from facies and lithological analysis (also see Barrett et al., this volume). "n"=non-glacial, "d"=ice distal, "p"=ice proximal and "i"= ice contact.

to no more than ~450 k.y., allowing the possibility of 100 k.y.-frequency sequences that may correspond to the eccentricity component of the Earth's orbit. Age Model B restricts the duration of the 3 sequences to ~120 k.y. period, and the frequency to ~40 k.y. per sequence, although shorter orbital (20 k.y.) and sub-orbital frequencies are also possible using this age model if time is missing at sequence boundaries.

Frequency analysis of depth series data

Spectra from harmonic analysis of 0.5-1.0m-spaced percent sand depth and time series spanning sequences 9, 10 and 11 (CRP-2/2A) are illustrated in Fig. 8. We have set $\lambda=0.4$ for Seigel's test since we

are looking for more than one Milankovitch periodic component in the data.

Visual inspection of depth series of percent sand for sequences 9, 10 and 11 shows marked cyclicality at the sequence scale as described above and illustrated in figure 5. Sequences 10 and 11 correspond to 2 discrete cycles in sand content. However, these 2 cycles of *c.* 40m thickness are superimposed on a larger *c.* 80m-thick cycle representing a sandstone to mudstone to sandstone succession between 185 and 300 mbsf. Sequence 9 comprises a sandstone-mudstone-sandstone cycle of *c.* 50 m thickness. Superimposed on sequence 9 are higher-frequency 10 m thick cycles in grainsize. Periodic components are

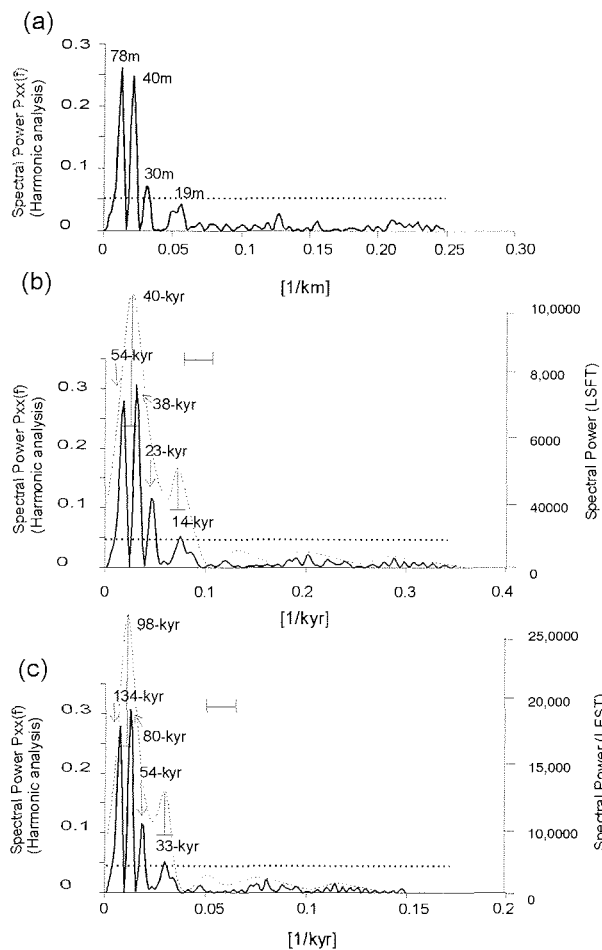


Fig. 8 - Harmonic analysis using Siegel's test to identify 1 or more periodic components from background noise in 0.5 to 1.0m-spaced percentage sand data (>56 μ m, Appendix 1) from CRP-2/2A sequences 9,10 and 11. (a) Depth data (Settings: OFAC=4; HIFAC=1; $\alpha=0.05$; $\lambda=0.4$; $T_\lambda = 0.362$, and $t_c=0.104$, thus $T_\lambda > t_c$). Amplitude of periodic components exceeds g_s (dashed line) at 78m, 40m and 30m. 6dB bandwidth = 0.0068. (b) Time series data calibrated by age model B (Fig. 4; $T=120$ k.y. Settings: OFAC=4; HIFAC=1; $\alpha=0.05$; $\lambda=0.4$; $T_\lambda = 0.486$, and $t_c=0.102$, thus $T_\lambda > t_c$). Amplitude of periodic components exceeds g_s (dashed line) at 54 k.y., 38 k.y., 23 k.y. and 14 k.y. frequency bands. Note that the smoothed LFST power spectrum (dashed curve) of the time series yields periodic components at 40 k.y. and 14 k.y. (Settings: OFAC=4; HIFAC=1; N_{seg} in WOSA=4; Hanning window). (c) Time series data calibrated by age model A (Fig. 4; $T=300$ k.y. Settings: OFAC=4; HIFAC=1; $\alpha=0.05$; $\lambda=0.4$; $T_\lambda = 0.486$, and $t_c=0.102$, thus $T_\lambda > t_c$). Amplitude of periodic components exceeds g_s (dashed line) at 134 k.y., 80 k.y., 54 k.y. and 33 k.y. frequency bands. Note that the smoothed LFST power spectrum (dashed curve) of the time series yields periodic components at 100 k.y. and 33 k.y. (Settings: OFAC=4; HIFAC=1; N_{seg} in WOSA=4; Hanning window).

detected in harmonic frequency spectra of percent sand at 78 m, 40 m, 30 m and 19 m. The 78 m and 40 m periodicities appear to correspond to the prominent sequence-scale grainsize variations (Fig. 8a).

Frequency analysis of time series data

Harmonic analysis of percent sand data for sequences 9-11 calibrated by age model A ($T=300$ k.y.) reveals statistically significant

components above noise levels at 134 k.y., 80 k.y., 54 k.y. and 33 k.y. (Fig. 8c), none of which correspond to Milankovitch orbital frequencies. However, given that the time series may contain a significant level of noise we ran a smoothing procedure (WOSA, with 3 overlapping segments and a Hanning Window). The resulting spectrum in figure 8c displays a statistically significant ($\alpha=0.2$) periodic component at 98 k.y. Such a result is not surprising given that age model A time series comprises 3 sequences/3 grainsize cycles, each of 100 k.y.

Harmonic analysis of percent sand data for sequences 9-11 calibrated by age model B ($T=120$ k.y.) reveals statistically significant components above noise levels at 54 k.y., 38 k.y., 23 k.y. and 14 k.y. (Fig. 8b). 54 k.y. and 38 k.y. peaks fall within the frequency range of the obliquity orbital parameter, known as axial tilt. 23 k.y. corresponds to one of the precessional frequencies. Given its low amplitude, the 14 k.y. peak may be spurious, but intriguingly, it is of similar duration to the time interval separating major ice-rafting events during the late Quaternary in the North Atlantic Ocean. We applied the same smoothing procedure (WOSA, with 3 overlapping segments and a Hanning Window) to age model B time series. The resulting spectra in figure 8b display a statistically significant ($\alpha=0.2$) periodic component at 40 k.y.. As for age model A time series, such a result is not surprising given that the time series comprises 3 sequences/3 grainsize cycles of 40 k.y. duration.

CRP-3

Age Model

The age model used to construct time series for sequences 1-7 is based on the $^{87}\text{Sr}/^{86}\text{Sr}$ analyses of molluscs (Lavelle, this volume), and correlation of a magnetic polarity zonation to the magnetic polarity time scale (Florindo et al., this volume, Hannah et al., this volume) (Fig. 4). Correlation of the magnetic polarity stratigraphy of this interval to the magnetic polarity timescale (MPTS) indicates that sequences 1-7 can correlate with the upper part of Chron C12Cr, which is supported by four $^{87}\text{Sr}/^{86}\text{Sr}$ ages spanning the stratigraphic interval. The four $^{87}\text{Sr}/^{86}\text{Sr}$ values all give the same statistical age blanketing the time interval of $\sim 30.9 \pm 1\%$ ma, and imply that the 230 m of section spanning sequences 1-7 accumulated very rapidly. Using the age of the top of C12Cr and the older limit of the uncertainty range of $^{87}\text{Sr}/^{86}\text{Sr}$ values as maximum constraints, we have assigned a maximum age range of 300 k.y. to sequences 1-7. Our age model implies that each sequence corresponds to a ~ 40 k.y.; the period of the obliquity orbital parameter.

Frequency analysis of depth series data

Spectra from harmonic analysis of 0.5m-spaced percent sand depth and time series spanning

sequences 1-7 (CRP-3) are illustrated in figure 9. Again, we have set $\lambda=0.4$ for Siegel's test since we are looking for more than one Milankovitch periodic component in the data. Visual inspection of depth series of percent sand for sequences 1-7 shows a marked cyclicity at the sequence scale as described above and illustrated in figure 4. Each sequence comprises a cycle of sand content represented by a sandstone-mudstone-sandstone succession. Significant periodic components are detected in the harmonic frequency spectrum (Fig. 9A) of percent sand at 218m, 62m, 32-26m, 22m, 17m and 9m.

Frequency analysis of time series data

Harmonic analysis of percent sand data for sequences 1-7 calibrated by our age model ($T=300$ k.y.) reveals statistically significant components above noise levels at 100 k.y., 41 k.y., 23-19 k.y., 15 k.y., 12 k.y. and 10 k.y. (Fig. 9b). The results are intriguing as the spectrum of Milankovitch orbital frequencies (100 k.y., 41 k.y., 23 k.y. and 19 k.y.) are present together with higher frequency components consistent with the duration between known Late Quaternary ice rafting episodes at the sub-orbital scale

of 15-10 k.y.. The 41 k.y. frequency contains the most power in the spectrum (Fig. 9b), followed by the precessional frequency bands, yet the time series appears to contain significant modulation by 100 k.y. eccentricity. Though, circular, it is tempting to suggest that our age model for sequences 1-7 is indeed accurate as the contained cyclicity of the time series matches the 3 main harmonic functions of the astronomical system which is responsible for Earth's climate and sedimentary cyclicity. A fundamental requirement of astronomical tuning of a sedimentary record to confirm or derive an age model is that the cyclicity observed within the stratigraphic record must be periodic and that the relationship to the astronomical forcing function must be (independently) provable. Though this is not possible to do with sequences 1-7 in CRP-3, Naish et al (2001) have demonstrated the existence of sequence-scale, orbitally-induced cyclicity for sequences 9, 10 & 11 in CRP-2/2A.

CYCLE DURATION AND PERIODICITY AT THE INTRA-SEQUENCE SCALE

SEQUENCE 11, CRP-2/2A

One hundred, 0.5 to 1.0m-spaced percent sand, grainsize determinations plotted against sequence 11 reveal two cycles, characterised by ice-proximal muddy-diamictite overlain by lower shoreface to inner shelf well-sorted sandstone, overlain again by offshore shelf mudstone, nearshore sandstone and ice proximal diamictite (Fig 10a). The observed cyclicity reflects the presence or absence of a mud component in ice proximal and ice distal facies. Environmental interpretations from facies analysis support a single cycle only, of ice advance-retreat-readvance and relative sea-level change. Harmonic spectral analysis was undertaken on percent sand data to identify periodic components above noise level within sequence 11. While we acknowledge that the data series is too short to yield reliable periodic components at the low-frequency end of the spectrum, a single periodic component above background noise level occurs at 34 m and represents spectral power due to the 2 cycles in sand content. Calibration of sequence 11 data to time series by age models A and B yielded a periodicity for the cycle of 55 k.y. (Fig. 10c) and 23 k.y. (Fig. 10b), respectively. The result is not surprising as age models A and B assign 100 k.y. and 40 k.y. to the duration of sequence 11, respectively. However, we re-emphasise that the two intrasequence cycles probably reflect a facies control characteristic of diamictic successions and should not necessarily be interpreted as 2 climate cycles.

SEQUENCE 2, CRP-3

Harmonic spectral analysis of 160, 0.5m-spaced percent sand data points from sequence 2, yielded

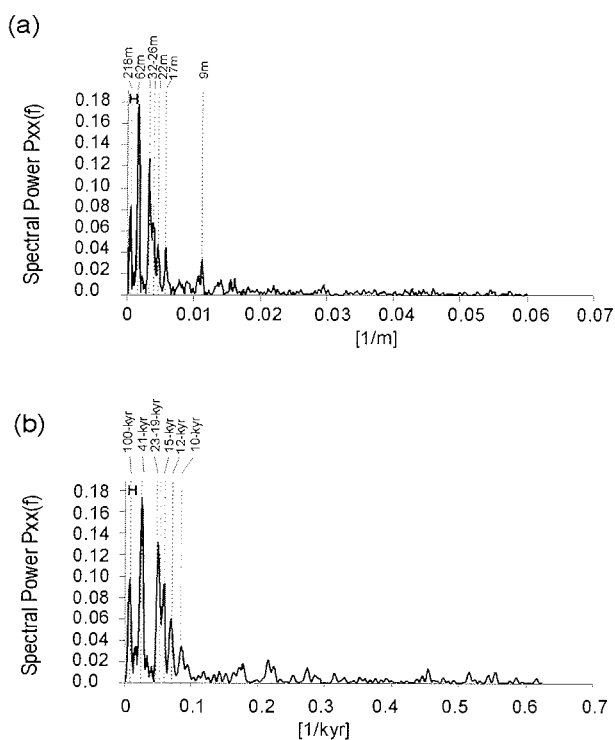


Fig. 9 - Harmonic analysis using Siegel's test to identify 1 or more periodic components from background noise in 0.5 m-spaced percentage sand data ($>56\mu\text{m}$, Appendix 1) from CRP-3 sequences 1 to 7. (a) Depth data (Settings: OFAC=4; HIFAC=1; $\alpha=0.05$; $\lambda=0.4$; $T_\lambda = 0.373$, and $tc=0.065$, thus $T_\lambda > tc$). Amplitude of periodic components exceeds gs (dashed line) at 218m, 62m and 32-26m, 22m, 17m and 9m. 6dB bandwidth = 0.0056. (b) Time series data calibrated by age model B (Fig. 4; $T=300$ k.y. Settings: OFAC=4; HIFAC=1; $\alpha=0.05$; $\lambda=0.4$; $T_\lambda = 0.380$, and $tc=0.065$, thus $T_\lambda > tc$). Amplitude of periodic components exceed gs (dashed line) at 100 k.y., 41 k.y., 23-19 k.y., 15 k.y., 12 k.y. and 10 k.y. frequency bands. 6dB bandwidth=0.032.

periodic components at 83m, 31m, and 20m (Fig. 11a). When calibrated to our age model these peaks revealed frequencies of 41 k.y., 19 k.y. and 10 k.y., respectively (Fig. 11b). The higher frequency components at 19 k.y. (orbital precession) and at 10 k.y. are superimposed on the 41 k.y. cycle. A number of smaller scale cycles in percent sand can be observed in Fig. 7, but are not significant above background noise level; i.e they fail Siegel's Test.

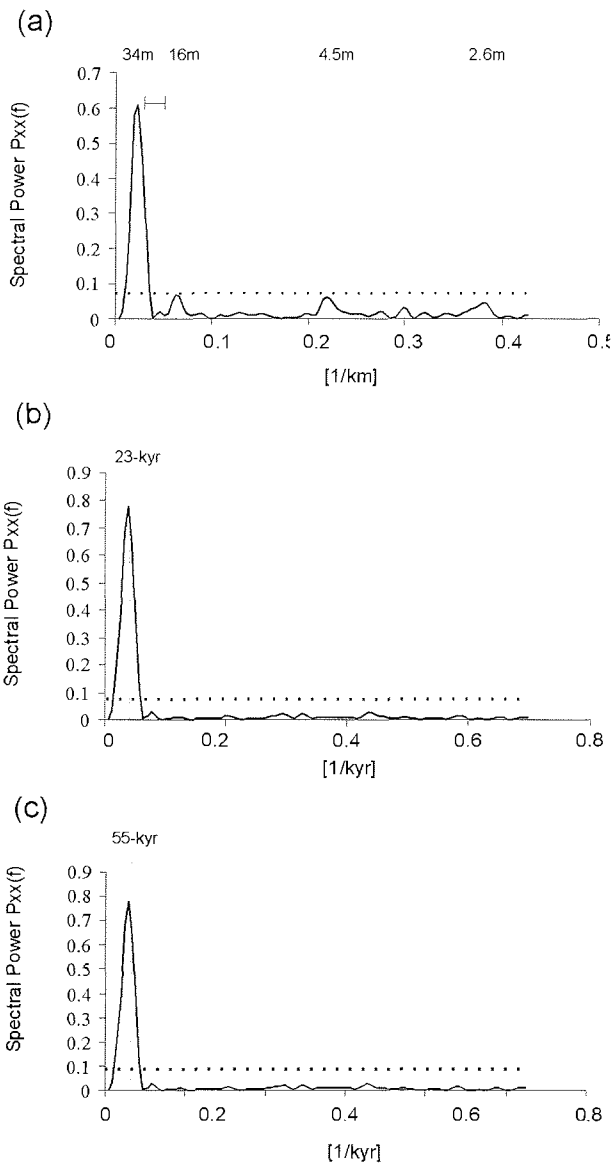


Fig. 10 - Harmonic analysis using Siegel's test to identify 1 or more periodic components from background noise in 0.5 to 1.0m-spaced, percentage sand data ($>56\mu\text{m}$, Appendix 1) from CRP-2/2A sequence 11 (Fig. 8). (a) Depth data (Settings: OFAC=4; HIFAC=1; $\alpha=0.05$; $\lambda=0.4$; $T_\lambda = 0.452$, and $t_c=0.181$, thus $T_\lambda > t_c$). Amplitude of periodic components exceeds g_s (dashed line) at 34m. 6dB bandwidth = 0.019. (b) Time series data calibrated by age model B (Fig. 4; $T=41$ k.y. Settings: OFAC=4; HIFAC=1; $\alpha=0.05$; $\lambda=0.4$; $T_\lambda = 0.642$, and $t_c=0.181$, thus $T_\lambda > t_c$). Amplitude of periodic components exceed g_s (dashed line) at 23 k.y. frequency band. (c) Time series data calibrated by age model A (Fig. 4; $T=100$ k.y.). Settings: OFAC=4; HIFAC=1; $\alpha=0.05$; $\lambda=0.4$; $T_\lambda = 0.642$, and $t_c=0.181$, thus $T_\lambda > t_c$). Amplitude of periodic components exceed g_s (dashed line) at 60 k.y. frequency band.

We contend that periodic components at the low-frequency end of intra-sequence spectra (Figs. 10 & 11) are real, as the same frequencies were observed with significant power in spectra generated for longer time series that included sequence 11, CRP-2/2A and sequence 2, CRP-3.

DISCUSSION

The analysis of periodicities within grain size data from CRP core contributes to an understanding of the frequency of oscillations in the size of the East Antarctic Ice Sheet. The nature of sedimentary cyclicity in the CRP drillcore has been evaluated at two different spatial and temporal levels:

Sequence-scale - 0.5-1.0m-spaced percentage sand depth and time series data spanning sequences 9-11 (128 to 306.65 mbsf; CRP-2/2A) and

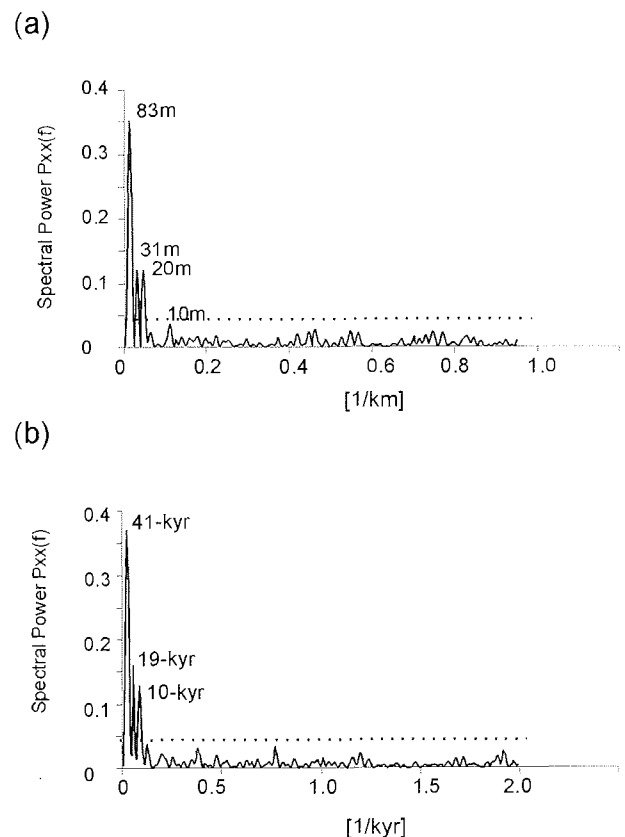


Fig. 11 - Harmonic analysis using Siegel's test to identify 1 or more periodic components from background noise in 0.5m-spaced, percentage sand data ($>56\mu\text{m}$, Appendix 2) from CRP-3 sequence 2 (Fig. 8). (a) Depth data (Settings: OFAC=4; HIFAC=1; $\alpha=0.05$; $\lambda=0.4$; $T_\lambda = 0.356$, and $t_c=0.105$, thus $T_\lambda > t_c$). Amplitude of periodic components exceeds g_s (dashed line) at 83m, 31m and 20m. 6dB bandwidth = 0.015. (b) Time series data (Fig. 4; $T=41$ k.y. Settings: OFAC=4; HIFAC=1; $\alpha=0.05$; $\lambda=0.4$; $T_\lambda = 0.383$, and $t_c=0.104$, thus $T_\lambda > t_c$). Amplitude of periodic components exceed g_s (dashed line) at 41 k.y., 19 k.y., and 10 k.y. frequency bands. 6dB bandwidth=0.03.

sequences 1-7 (13.0 to 230.0 mbsf; CRP-3). Sedimentary cycles of ice margin advance-retreat-readvance in concert with relative water depth changes range from 5 to 80m thickness and correspond in duration to Milankovitch orbital periodicities; eccentricity (*c.* 100 k.y.) using age model A (sequences 9-11, CRP-2/2A), and obliquity (*c.* 41 k.y.) using age Model B (sequences 9-11, CRP-2/2A) and age model for sequences 1-7, CRP-3).

Intrasequence-scale - 0.5-1.0m-spaced percentage sand depth and time series data spanning two characteristic vertically-stacked facies successions; sequence 11 (CRP-2/2A) and sequence 2 (CRP-3). Smaller scale intrasequence percent sand cycles ranging from *c.* 10-40 m thickness correspond to spurious non-orbital frequencies using age model A, and precessional orbital (19 & 23 k.y.) and sub-orbital bandwidths (15-10 k.y.) using age model B.

IMPLICATIONS FOR ORBITAL CONTROL OF THE EAST ANTARCTIC ICE SHEET DURING THE LATE OLIGOCENE-EARLY MIOCENE

The astronomical system responsible for climate and sedimentary cyclicality contains three main harmonic functions, referred to as eccentricity, obliquity and precession. Each of these functions consists of a complex frequency spectrum, but as a first approximation, their average periodicities are 20 k.y. for precession, 40 k.y. for obliquity and 100 k.y., 400 k.y. and 2000 k.y. for eccentricity. Theoretically, the obliquity signal changes the latitudinal distribution of incident solar radiation and is more significant at higher latitudes. Eccentricity modulates the amplitude of the precession and thus influences the total annual/seasonal solar energy budget and has its most profound effect on seasonal insolation at low latitudes (Berger & Loutre, 1994). The causal link between astronomical-forcing of climate and sedimentation has been well-established since the work of Hays et al. (1976) on deep-sea benthic $\delta^{18}\text{O}$ records, yet the exact origin of the orbital control at the 100 k.y. frequency band remains contentious (summarised in Paul & Berger, 1999). Eccentricity of Earth's orbit around the sun, or periodic variations of inclination of Earth's ecliptic (Muller & MacDonald, 1997) have been proposed as possible mechanisms. Furthermore, the 100 k.y. orbital frequency has been shown for the Pleistocene ice ages to be "too small in amplitude and too late in phase to produce the corresponding climate cycle by direct forcing" (Imbrie et al., 1993; p. 700). Intriguingly, the 100 k.y. frequency lacks power in pre-Pleistocene climate proxy records (Zachos et al., 1996, Paul et al., 2000), and in orbital insolation

solutions (Laskar et al. 1993; Shackleton et al., 1999). On the other hand the 41 k.y. obliquity cycle, which is attributed to axial-tilt, has been shown to exercise a strong influence on high latitude insolation, and thereby is considered to play the major orbital control on the stability of large continental ice sheets. Notwithstanding this, certain intervals of early Cenozoic oxygen isotope records (Late Oligocene-Early Miocene; Paul et al., 2000) do contain 100 k.y. cycles.

Previously recovered glacial marine sediments on, or near, the Antarctic margin imply that grounded ice has covered much of Antarctica since the earliest Oligocene (Hays et al., 1975; Kennett, 1977; Barrett, 1986; Barrett et al., 1987; Barrett, 1989; Barron et al., 1989; Schlich et al., 1989; Hambrey et al., 1991; Wise et al., 1991). This evidence is consistent with the benthic foraminiferal oxygen isotope records from the southern ocean, which show a ubiquitous increase of $> 1.0\%$ coeval with a period of widespread ice rafting at 33.5Ma (*e.g.* Shackleton & Kennett, 1975; Kennett & Shackleton, 1976; Keigwin, 1980; Miller & Thomas, 1985, Zachos et al. 1992, 1996; 1997).

While a unipolar "ice house" world is widely accepted for the Oligocene, several lines of evidence suggest progressive climatic amelioration of Antarctica during the mid- to late Oligocene/Early Miocene, and that waning ice sheets alternated with periods of more intense glaciation (Stott et al., 1990; Miller et al., 1991; Wright & Miller, 1992). The nature of these inferred oscillations is poorly understood, because previously cored Antarctic margin sedimentary records, have been hampered by poor core recovery, large stratal hiatus, and a lack of chronological detail needed to resolve palaeoenvironmental changes on time scales of $< 10^5$ years.

Spectral analyses of CRP-2/2A data calibrated to age model B, and CRP-3 data, indicates that mid-Cenozoic sequence-scale oscillations are forced by the obliquity component. This result is consistent with the insolation frequency spectrum for the Oligocene-Miocene (Shackleton et al., 1999). Moreover, coeval high-resolution oxygen isotope time series from ODP site 929 on the Ceara Rise (Zachos et al., 1997) are dominated by high-amplitude obliquity cycles with modulation of the obliquity signal by 400 k.y. eccentricity, not the 100 k.y. component. Thus, although age model A for sequences 9-11 in CRP-2/2A does allow 100 k.y. orbital influence, our age model for the upper part of CRP-3 does not allow 100 k.y. cyclicality for sequences 1-7. Detailed time series analysis of ODP site 929 benthic oxygen isotope record on the Ceara Rise shows that several ~ 100 k.y. cycles punctuate the obliquity-dominated earliest Miocene interval following the Mi-1 glacial excursion (Paul et al., 2000). This may be consistent with the 100 k.y. cyclicality inferred from age model A.

CONCLUSIONS

Given a causal link between astronomical-forcing of climate and ice volume, we contend that sedimentary cyclicity in the CRP core was induced by ice margin fluctuations and coeval changes in glacioeustatic sea level. The most dynamic fluctuations in the ice margin and water depth are manifest as large-scale sequences, which represent cycles of advance and retreat of grounded glacier ice across the Ross Sea continental shelf. Cyclical changes in water depth occurred concomitantly from shoreline-inner shelf to outer shelf water depths (c. 50 m magnitude). These local relative water depth changes resulted from the combined influence of eustasy, local tectonism, isostasy, and sediment supply. The isolation of the eustatic sea-level component from a continental-margin sedimentary succession is inherently difficult to achieve (e.g. Naish, 1998). Given present data it is not yet possible to estimate the amplitude of any glacio-eustatic component. However, the inferred changes in water depth illustrated in figures 3 & 5 are consistent with the magnitude of eustatic water depth changes inferred for the Oligocene-Miocene from seismic records (Haq et al. 1987; Abreu & Anderson, 1998), and deep ocean oxygen isotope records (Zachos et al. 1996; Zachos et al., 1997).

The small scale changes of ice margin proximity, ice berg rafting, melt water discharge and/or relative sea-level that we have inferred at the intrasequence scale could have been influenced by precession, and sub-Milankovitch climate change. Age model A implies a significant hiatus at the sequence 9/10 boundary, and if correct may provide the first direct evidence of a major glaciation at the Oligocene-Miocene boundary predicted by the Mil event in distal $\delta^{18}\text{O}$ records. Alternatively, age Model B implies that the Mil event corresponds to the sequence 8/9 boundary, another significant erosional unconformity in CRP-2/2A.

SUMMARY

Our sequence stratigraphic analysis supports earlier suggestions that nearshore marine strata beneath the Antarctic continental shelf record fluctuations in the size of the EAIS. Individual sequences in CRP core record cycles of advance, retreat, and re-advance of the ice margin by tens of kilometres across the western Ross Sea continental shelf, in concert with relative water depth variations of up to 50 m. Our chronological data, supported by spectral analysis for sequences 9-11 (CRP-2/2A) and sequences 1-7 (CRP-3), suggest that these sequences had durations of similar length to Milankovitch frequencies, probably 41 k.y., but possibly as low as 100 k.y.. We conclude that the cyclicity recorded by glacial marine sequences

in the CRP drillcore provides strong evidence for orbitally-induced oscillations in the size of the Oligocene EAIS, analogous to those that occurred later in the Quaternary northern hemisphere ice sheets.

ACKNOWLEDGEMENTS - The Cape Roberts Project was made possible by the resources and close collaboration of the Antarctic programmes of Italy, New Zealand, United States of America, Germany, Australia, Great Britain, and The Netherlands with field operations organised by Antarctica New Zealand. We gratefully acknowledge the efforts of the Cape Roberts Project International Steering Committee, the Operations/Logistics Management Group, as well as the drilling, logistic support and science teams whose hard work and enthusiasm provided the material on which this paper is based. The authors also acknowledge the support of their home institutions and national funding agencies.

REFERENCES

- Abbott S.T. & Carter R. M., 1994. The sequence architecture of mid-Pleistocene (ca. 1.1-0.4 Ma) cyclothems from New Zealand: facies development during a period of orbital control on sea level cyclicity. In: de Boer, P. L. and Smith, D. G. (eds), *Orbital Forcing and Cyclic Sequences*, pp. 367-394. International Association of Sedimentologists Special Publication, 19.
- Abreu V. & Anderson J. B., 1998. Glacial Eustasy during the Cenozoic: Sequence Stratigraphic Implications, *AAPG Bulletin*, 82, 1385-1400.
- Barrett P. J. (ed). 1986. Antarctic Cenozoic history from MSSTS-1 drillhole, McMurdo Sound. *DSIR Bulletin*, 245, 251pp.
- Barrett P.J., 2001. Grain-size analysis of samples from CRP-3, Victoria Land Basin, Antarctica, with inferences about depositional setting and environment. This volume.
- Barrett P.J., Elston D.P., Harwood D.M., McKelvey B.C. & Webb P.-N. 1987. Mid-Cenozoic record of glaciation and sea-level change on the margin of the Victoria Land basin, Antarctica, *Geology*, 15, 634-637.
- Barrett P.J. (ed). 1989. Antarctic Cenozoic history from CIROS-1 drillhole, McMurdo Sound. *DSIR Bulletin*, 245, 251pp.
- Barrett P.J. & Anderson J., 2000. Grainsize analysis and preliminary interpretation from CRP-3, Victoria Land Basin, Antarctica, *Terra Antarctica*, 7, 373-378.
- Barron J.A., et al. (eds). 1989. *Proceedings of the Ocean Drilling Programme Initial Report*, 119, Ocean Drilling Programme, College Station, Texas.
- Berger A. & Loutre M.F., 1994. Astronomical forcing through geological time, in de Boer, P.L. & Smith, D. G. (eds.) *Orbital Forcing and Cyclic Sequences*, *Special Publication, International Association of Sedimentologists*, 19, 15-24.
- Blackman R.B. & Tukey J.W., 1958, *The measurement of power spectra from the point of view of communication engineering*, Dover Publications, New York. 190p.
- Cape Roberts Science Team, 1999. Studies from the Cape Roberts Project, Ross Sea, Antarctica, Initial report on CRP-2/2A, *Terra Antarctica*, 6, 1-173.
- Cape Roberts Science Team, 2000. Studies from the Cape Roberts Project, Ross Sea, Antarctica, Initial report on CRP-3, *Terra Antarctica*, 7, 1-209.
- Cande S.C. & Kent D.V., 1995. Revised calibration of the geomagnetic polarity time scale for the Late Cretaceous and Cenozoic. *Journal of Geophysical Research*, 100, 6093-6095.
- Fielding C.R., Naish T.R., Woolfe K.J., & Lavelle M., 2000, Facies Analysis and Sequence Stratigraphy of CRP-2/2A, McMurdo Sound, Antarctica, *Terra Antarctica*, 7, 323-338.

- Fielding C.R., Dunbar G.B. & Bryce S.M., 2001. Laser-Derived Particle Size Data from CRP-3, Victoria Land Basin, Antarctica: Implications for Sequence and Seismic Stratigraphy. This volume.
- Fielding C.R., Naish T.R. & Woolfe K.J., 2001. Facies Analysis and Sequence Stratigraphy of CRP-3, Victoria Land Basin, Antarctica. This volume.
- Florindo et al., 2001. Magnetostratigraphy of CRP-3, Victoria Land Basin, Antarctica. This volume.
- Hannah M. et al., 2001. Chronology of CRP-3, Victoria Land Basin, Antarctica. This volume.
- Hambrey M.J., Ehrmann W.U., & Larsen B. 1991. Cenozoic glacial record of the Prydz Bay continental shelf, East Antarctica. *Proceedings of the Ocean Drilling Program Initial Reports*, **119**, 77-132, Ocean Drilling Programme, College Station, Texas.
- Haq B.U., Hardenbol J. & Vail P.R., 1987. Chronology of fluctuating sea-levels since the Triassic, *Science*, **235**, 1156-1167.
- Hays J.D., Imbrie J. & Shackleton N.J., 1976. Variations in Earth's Orbit: Pacemaker of the ice ages, *Science*, **194**, 1121-1132.
- Hays D.E., Frakes L.A., et al., 1975. *Initial reports of the Deep Sea Drilling Project 29*, Washington D.C., U.S. Government printing office.
- Henrys S.A., Bücker C.J., Bartek L.R., Bannister S., Niessen F. & Wonik T., 2000. Correlation of seismic reflectors with CRP2/2A, Victoria Land Basin, Antarctica. *Terra Antarctica*, **7**, 221-230.
- Imbri, J. and 19 others, 1993. On the structure and origin of major glaciation cycles 2. The 100,000 year cycle. *Palaeoceanography*, **8**, 699-735.
- Jenkins G.M. & Watts D.G. (1968) *Spectral Analysis and its Application*. Holden-day, Oakland, 525pp.
- Keigwin L.D., 1980. Palaeoceanographic change in the Pacific at the Eocene-Oligocene boundary, *Nature*, **287**, 722-725.
- Kennett J.P., 1977. Cenozoic evolution of Antarctic glaciation, the circum-Antarctic Ocean and their impact on global palaeoceanography. *Journal of Geophysical Research*, **82**, 3843-3860.
- Kennett J.P. and Shackleton N.J., 1976. Oxygen isotope evidence for the development of the cryosphere 38 m.y. ago, *Nature*, **260**, 513-515.
- Laskar J., Joutel F. & Boudin F., 1993. Orbital, precessional and insolation quantities for the Earth from -20Myr to +20Myr. *Astronomy and Astrophysics*, **270**, 522-533.
- Lavelle M., 2000. Strontium isotope stratigraphy and age model for CRP-2/2A, Victoria Land Basin, Antarctica. *Terra Antarctica*, **7**, 611-620.
- Lavelle M., 2001. Strontium isotope stratigraphy and age model for CRP-3, Victoria Land Basin, Antarctica. This volume.
- Lomb N.R., 1976. Least-squares frequency analysis of unequally spaced data. *Astrophysics and Space Science*, **39**, 447-462.
- Milankovitch V., 1995. *Milutin Milankovic, from his autobiography by his son, Vasko and a preface by Andre Berger*. Katlenburg-Lindau: European Geophysical Society.
- Miller K.G., Wright J.D. & Fairbanks R.G. 1991. Unlocking the ice house: Oligocene oxygen isotopes, eustasy and margin erosion. *Journal of Geophysical Research* **96**, 6829-6848.
- Miller K.G. & Thomas E., 1985. Late Eocene to Oligocene benthic foraminifera isotope record, site 574, equatorial Pacific. *Initial report of the Deep Sea Drilling project*, **85**, 771-777.
- Muller R.A. & MacDonald G.J., 1997. Simultaneous presence of orbital inclination and eccentricity in proxy climate records from Ocean Drilling Program Site 806. *Geology*, **25**, 3-6.
- Naish T.R. & Kamp P.J.J., 1997. Sequence stratigraphy of 6th order (41 k.y.) Pliocene-Pleistocene cyclothems, Wanganui Basin, New Zealand: A case for the regressive systems tract. *Geological Society of America Bulletin*, **109**, 978-999.
- Naish T.R., Abbott S.T., Alloway B.V., Beu A.G., Carter R.M., Edwards A.R., Journeaux T.D., Kamp P.J.J., Pillans B., Woolfe K., 1998. Astronomical Calibration of a Southern Hemisphere Plio-Pleistocene Reference Section, Wanganui Basin (New Zealand). *Quaternary Science Reviews*, **17**, 695-710.
- Naish T.R., 1998. Constraints on the amplitude of late Pliocene eustatic sea-level fluctuations: New evidence from the New Zealand shallow-marine sediment record. *Geology*, **25**, 1139-1142.
- Naish T.R., Woolfe K.J., Barrett P.J., Wilson G.S., Atkins C., Bohaty S.M., Bucker C., Claps M., Davey F., Dunbar G., Dunn A., Fielding C.R., Florindo F., Hannah M., Harwood D.M., Watkins D., Henrys S., Krissek L., Lavelle M., van der Meer J.J.P., McIntosh M.C., Niessen F., Passchier S., Powell R., Roberts A.P., Sagnotti L., Scherer R.P., Strong C.P., Talarico F., Verosub K.L., Villa G., Webb P-N., & Wonik T. 2001. Orbitally-induced oscillations in the East Antarctic Ice Sheet: Direct evidence from Antarctic margin drilling. *Nature*, **413**, 719-723.
- Paul H.A., Zachos J.C., Flower B.P. & Tripathi, 2000. Orbitally induced climate and geochemical variability across the Oligocene/Miocene boundary. *Palaeoceanography*, **15**, 471-485.
- Paul A. & Berger W., 1999. Climatic cycles and climatic transitions as a response to astronomical and CO2 forcings. in (eds.) Harff J., Lemke W. and Statterger K., *Computerized Modeling of Sedimentary Systems*, Springer, Heidelberg, 452 p.
- Percival D.B. & Walden A.T., 1993. *Spectral Analysis for Physical Applications*. Cambridge University Press, Cambridge, 583 pp.
- Powell R.D., 1981. A model for sedimentation by tidewater glaciers. *Annals of Glaciology*, **2**, 129-134.
- Powell R.D., Krissek L.A. and van der Meer J.M., 2000. Depositional environments of Cape Roberts 2/2A Drill Core. *Terra Antarctica*, **7**(3), 313-322.
- Powell R.D., Laird M.G., Naish T.R., Fielding C.R., Krissek L.A. & van der Meer J.M., this volume. Depositional environments for strata cored in CRP-3, Victoria Land Basin, Antarctica, Palaeoglaciological and palaeoclimatological implications.
- Sandroni S. & Talarico F., 2001. Variability, petrography and provenance of basement clasts in core from CRP-3. Victoria Land Basin, Antarctica. This volume.
- Scargle J.D., 1982. Studies in astronomical time series analysis II. Statistical aspects of spectral analysis of unevenly spaced data. *The Astrophysical Journal*, **263**, 835-853.
- Scargle J.D., 1989. Studies in astronomical time series III. Fourier transforms, autocorrelation function, and cross-correlation of unevenly spaced data. *The Astrophysical Journal*, **343**, 874-887.
- Schlich R., et al., 1989. *Proceedings of the Ocean Drilling Program Initial Reports*, **120**, Ocean Drilling Programme, College Station, Texas.
- Shackleton N.J. & Kennett J.P., 1975. Palaeotemperature history of the Cenozoic and the initiation of the Antarctic glaciation, oxygen and carbon isotope analyses in DSDP Sites 277, 279 and 281. *Initial report of the Deep Sea Drilling project*, **29**, 743-755.
- Shackleton N.J., Crowhurst S.J. Weedon G.P. and Laskar J. 1999. Astronomical (Milankovitch) calibration of the geological timescale. Astronomical calibration of the Oligocene-Miocene timescale. *Transactions of the Royal Society A*, **357**, 1907-1929.
- Shackleton N.J., 2000. The 100,000 year ice-age cycle identified and found to lag temperature, carbon dioxide and orbital eccentricity. *Science*, **289**, 1897-1902.
- Shackleton N.J., Hall M.A., Raffi I., Tauxe L. & Zachos J., 2000. Astronomical calibration for the Oligocene-Miocene boundary. *Geology*, **28**, 447-450.
- Schwarzacher M., 1999. Milankovitch cycles and sequences: Two different stratigraphic tools. In: Harff J., Lemke W. & Statterger K. (eds). *Computerised modelling of sedimentary systems*, Springer-Verlag Berlin Heidelberg, **224-247**.
- Shulz M. & Statterger K., 1997. Spectrum: Spectral analysis of unevenly spaced palaeoclimatic time series. *Computers & Geosciences*, **23**, 929-945.
- Siegel A.F., 1980. Testing for periodicity in time series. *Journal of the American Statistical Association* **75**, 345-348.
- Stott L.D., Kennett J.P., Shackleton N.J. & Corfield R.M., 1990. The evolution of Antarctic surface waters during the Palaeogene, inferences from stable isotope composition of planktonic foraminifera, *Proc. ODP Sci. Res.* **113**, 849-864.
- Vail P., 1987. Seismic stratigraphy interpretation using sequence stratigraphy, part 1: seismic stratigraphy interpretation procedure. In: Bally A.W., (ed.), *Atlas of Seismic Stratigraphy*:

- AAPG, Tulsa, Oklahoma, 27, 1-10.
- Welch P. D. 1967. The use of fast Fourier transform for the estimation of power spectra: A method based time averaging over short, modifies periodograms. *IEEE Transactions on Audio and Electroacoustics*, 15, 70-73.
- Wilson G.S., Bohaty S.M., Fielding C.R., Florindo F., Hannha M.J., Harwood D.M., McIntosh W.C., Naish T.R., Roberts A.P., Sagnotti L., Scherer R.P., Strong C.P., Verosub K.L., Villa G., Watkins D.K., Webb P.-N. & Woolfe K.J., 2000. Chronostratigraphy of the CRP-2/2A Drillhole, Ross Sea, Antarctica, *Terra Antarctica*, 7(4), 647.
- Wise S.W., Breza J.R., Harwood D.M., Wei W., 1991. Palaeogene glacial history of Antarctica. *Controversies in Modern Geology*, 133-177, Academic, San Diego.
- Wright J.D. & Miller K.G., 1992. Miocene stable isotope stratigraphy, Site 474, Kerguelen Plateau, *Proc. ODP Sci. Res.* 120, 855-866.
- Woolfe K.J., Fielding C.R., Howe J.A., Lavelle M. & Lally J.H., 1998. Laser-derived, particle size characterisation of CRP-1, McMurdo Sound, Antarctica, *Terra Antarctica*, 5(3), 383-392.
- Woolfe K.J., Stewart L.K., Fielding C.R. & Lavelle M., 2000. Laser-Derived, Particle Size Data from CRP-2/2A: Implications for Sequence and Seismic Stratigraphy, *Terra Antarctica*, 7(3), 369-372.
- Zachos J.C., Breza J., Wise S. W. Early Oligocene ice-sheet expansion on Antarctica, Sedimentological and isotopic evidence from Kerguelen Plateau, *Geology*, 20, 569-573 (1992).
- Zachos J.C., Quinn T.M., Salamy K.A., 1996. High-resolution deep-sea foraminiferal stable isotope records of the Eocene-Oligocene climate transition, *Palaeoceanography*, 11, 256-266.
- Zachos J.C., Flower B.P. & Paul H., 1997. Orbital paced climate oscillations across the Oligocene/Miocene boundary. *Nature*, 388, 567-570.

Appendix 1 - Percentage sand, mean grainsize, standard deviation and modal data for CRP-2/2A from 128.72 to 305.65 mbsf (Sample spacing = 0.5-1.0 m).

Depth (mbsf) Top interval	%Sand (>56um)	Mean	Standard deviation	Mode	Depth (mbsf) Top interval	%Sand (>56um)	Mean	Standard deviation	Mode
128.72	44.43	98.05	117.52	349	177.44	12.16	26.11	33.39	38
129.99	26.99	45.21	58.9	50	178.76	12.53	26.93	33.26	37
131.68	27.47	42.4	49.66	57	179.48	15.71	30.15	34.4	41
132.08	42.98	59.28	55.62	89	180.71	12.41	27.95	37.5	35
133.28	68.79	92.32	65.65	106	181.69	9.28	23.8	31.38	27
134.7	21.31	35.9	40.44	46	182.69	10.84	26.37	36.15	26
134.7	21.33	36.16	40.98	46	183.81	61.31	110.13	95.13	178
135.2	26.97	41.92	44.13	52	184.46	53.54	87.49	84.31	132
136.29	40.66	54.46	49.75	70	185.49	70.13	99.2	68.68	117
137.18	43.62	57.19	51.6	74	186.76	90.03	200.37	84.14	225
138	32.65	46.33	44.59	60	187.74	71.45	120.4	83.31	166
138.36	12.95	27.76	39.45	38	188.94	88.29	160.95	74.58	178
140.34	11.61	26.15	39.8	2	190.43	86.43	145.04	72.09	164
141.48	9.92	24.57	36.23	26	191.53	87.89	146.66	74.19	163
142.61	20.34	37.22	48.23	44	192.46	81.47	118.74	66.37	137
143.37	31.99	53.27	65.04	53	193.47	49.91	82.11	81.14	127
144.28	58.77	82.8	70.96	107	194.72	52.71	68.97	56.91	89
145.38	22.93	39.61	48.14	45	195.88	40.5	58.29	59.5	73
146.68	83.1	126.64	77.54	124	196.71	45.62	63.19	58.97	78
147.8	17.51	33.73	30.93	44	197.91	41.23	56.94	54.7	73
148.26	17.76	33.23	49.45	2	198.84	40.79	56.1	53.49	70
151.05	0.93	8.07	14.04	2	200.03	43.87	58.66	53.17	76
151.5	85.21	130.18	76.34	130	200.88	41.16	57.12	55.18	72
153.33	85.19	110.58	55.9	117	201.75	38.79	56.46	58.1	66
154.15	55	95.39	94.56	107	203.1	47.45	64.46	58.43	85
155.3	14.6	27.64	33.45	45	203.88	39.54	56.35	56.55	67
156.67	10.44	24.37	32.85	38	204.94	48.85	67.59	60.79	75
157.1	0.59	10.77	11.79	2	205.99	48.32	85.11	86.56	58
158.81	2.84	15.93	32.62	2	207	34	54.1	61.7	56
159.75	4.93	17.61	24.19	2	207.75	33.97	52.6	57.49	56
160.51	6.98	20.52	28.48	2	208.86	35	52.15	55.71	62
161.42	5.4	17.7	27.34	2	209.8	46.08	65.99	61.59	79
163.6	5.73	18.8	26.6	2	211.01	34.78	50.79	54.08	75
164.78	4.44	17.52	23.24	2	212	29.19	45.9	50.98	52
165.53	3.91	16.44	23.7	2	213.1	29.67	47.39	55.72	53
166.39	8.79	21.98	29.2	2	214.28	36.38	49.54	45.4	64
167.39	6	19.57	25.52	27	215.27	29.88	44.81	48.76	58
168.75	10.89	22.87	31.11	2	216.12	44.89	66.09	63.76	113
169.75	10.97	24.58	30.95	37	217.27	24.14	39.2	44.63	51
170.51	13.17	27.26	34.94	39	218.28	29.48	45.4	49.79	54
171.68	9.82	23.63	32.24	34	219.26	28.95	44.02	47.53	55
172.41	9.77	22.61	28.68	38	220.05	31.45	43.51	41.53	61
173.96	6.13	18.33	24.83	2	221.13	21.02	34.45	37.18	49
174.48	5.51	18.22	25.76	2	222.11	27.69	38.91	37.57	60
175.6	11.3	25.2	31.78	39	222.11	27.69	38.91	37.57	60
176.93	11.33	25.41	31.64	35	223.13	44.03	66.03	64.49	88

Appendix 1 - Continued

Depth (mbsf) Top interval	%Sand (>56µm)	Mean	Standard deviation	Mode	Depth (mbsf) Top interval	%Sand (>56µm)	Mean	Standard deviation	Mode
223.13	44.03	66.03	64.49	88	265.48	9.11	21.01	33.76	2
224.4	49.77	64.13	53.25	87	266.22	7.23	19.47	32.2	2
225.5	44.73	59.53	52.07	68	268.5	12.51	25.85	37.39	2
226.33	23.46	35.61	26.97	54	269.41	14.72	27.97	35	41
227.66	21.01	37.91	53.73	46	270.37	36.93	53.27	55.93	71
227.66	21.01	37.91	53.73	46	271.23	30.17	41.28	40.93	71
228.18	34.44	48.15	47.03	61	272.19	58.48	90.7	77.94	137
229.26	47.15	66.16	60.45	100	273.11	53.95	80.48	72.74	125
230.14	33.7	43.9	34.22	62	274.15	45.35	65.29	66.1	111
231.33	24.91	39.15	40.01	50	275.09	80.59	113.71	61.36	141
232.35	28.79	43.33	47.14	57	276.35	83.64	139.91	77.58	161
233.11	21.88	35.37	41.57	49	277.45	80.51	132.57	77.34	159
233.11	21.88	35.37	41.57	49	278.31	76.79	124.12	78.81	156
234.4	30.08	54.96	74.72	50	278.96	79.97	141.13	86.58	166
235.42	20.67	36.39	47.85	47	280.49	87.85	165.58	79.63	181
236.12	24.37	44.11	63.11	47	280.99	89.76	167.72	74.81	179
237.27	24.55	41.25	53.08	50	282.54	85.91	158.1	77.45	176
238.28	14.37	25.96	28.58	43	285.74	92.41	179.42	74.78	190
239.22	26.11	49.14	71.7	48	286.55	88.33	195.81	84.26	223
240.3	29.4	53.14	73.08	51	287.67	82.21	130.05	73.04	154
241.24	30.16	58.29	82.78	51	289	88.93	155.26	73.31	168
243.06	37.61	57.04	61.41	63	289.76	89.05	160.37	72	174
244.19	28.39	42.34	42.57	54	290.77	83.34	122.06	68.31	136
245.3	32.94	49.24	52.15	58	291.71	56.95	75.25	61.57	99
246.55	27.13	42.24	48.11	53	292.64	55.89	84.6	75.59	131
247.27	46.99	62.44	54.88	87	293.91	82.44	126.6	69.08	147
248.18	21.56	35.31	38.85	49	294.51	85.49	133.31	65.78	152
249.12	28.07	41.57	43.29	57	295.9	23.12	38.16	49.83	51
250.17	15.64	30.2	23.52	48	296.89	47.19	69.4	68.66	87
251.15	18.08	33.54	38.47	43	297.94	39.21	72.59	90.48	61
252.09	15.2	27.78	34.45	45	299.15	39.55	60.9	67.5	68
255.16	2.09	11.73	19.28	2	300.11	41.55	68.07	81.84	78
256.05	3.1	13.28	16.02	2	301.03	54.37	102.11	110.17	75
258.22	1.84	11.41	23.1	2	302.05	35.08	67.01	87.07	52
259.25	4.03	14.92	30.82	2	303.11	51.7	93.48	97.27	90
260.28	5.8	17.05	29.81	2	303.55	70.82	138.83	113.53	194
261.27	3.41	15.21	22	2	304.67	32.23	52.29	67.1	60
264.33	20.96	36.4	55.54	2	305.65	37.07	56.22	60.83	58

Appendix 2 - Percentage sand, mean grainsize, standard deviation and modal data for CRP-3 from 13 to 230 mbsf (Sample spacing = 50 cm).

Depth (mbsf) Top interval	%Sand (>56µm)	Mean	Standard deviation	Mode	Depth (mbsf) Top interval	%Sand (>56µm)	Mean	Standard deviation	Mode
13	23.76	42.38	60.2	48	24.5	58.69	105.31	103.15	117
13.5	43.79	71.2	80.62	80	25	22.52	44.7	70.53	2
14	37.29	60.86	76.14	75	26	6.98	23.56	19.99	38
14.5	27.22	51.59	76.28	2	26.5	52.96	89.13	90.96	116
15	34.09	66.13	90.09	9	27	81.8	174.3	112.05	234
15.5	30.49	57.01	79.75	2	28	59.07	103.68	98.07	134
16	32.41	60.69	82.9	2	28.5	61.19	113.7	105.83	178
16.5	10.6	25.47	49.48	2	29	22.34	35.76	48.66	57
17.5	50.23	59.56	47.83	71	29.5	45.2	70.91	78.58	79
18	19.8	32.99	50.94	2	30	15.25	30.45	51.08	2
18.5	34.67	56.68	72.44	2	30.5	50.55	78.07	80.8	91
19	10.64	21.76	35.06	2	31.1	30.97	49.68	64.23	59
19.5	33.92	47.61	59.03	72	31.5	36.24	52.67	61.47	64
20	35.01	56.29	72.04	66	32	23.29	36.37	52.54	2
21	32.17	48.69	56.87	57	32.5	30.14	45.39	59.37	68
21.5	34.92	60.3	80.06	2	33	12.12	26.51	50.39	2
22	45.96	82.03	93.6	98	33.5	15.27	32.83	59.24	2
22.5	50.18	90.66	97.37	227	34	15.22	31.69	56.31	2
23	53.83	97.95	101.81	156	34.5	9.25	25.17	21.33	40
23.5	20.2	36.08	58.56	2	35	14.77	29.92	48.71	2
24	59.79	107.07	103.1	119	35.5	13.36	30.19	53.99	2

Appendix 2 - Continued

Depth (mbsf) Top interval	%Sand (>56um)	Mean	Standard deviation	Mode	Depth (mbsf) Top interval	%Sand (>56um)	Mean	Standard deviation	Mode
36	9.01	22.3	38.3	2	68.5	9.03	19.73	33.95	2
36.5	4.9	16.55	30.26	2	69	5.81	15.9	30.11	2
37	10.43	23.72	43.21	2	69.5	7.26	18.64	36.03	2
37.5	13.56	33.77	66.87	2	70	9.78	26.05	63.05	2
38	13.01	29.48	54.71	2	70.5	8.56	21.13	39.56	2
38.5	10.69	27.59	54.54	2	71	6.81	16.54	24.14	2
39	12.72	30.4	57.01	2	71.5	0.28	7.26	8.81	2
39.5	10.57	26.1	50.96	2	72	43.75	52.23	47.87	85
40	14.8	32.35	57.3	2	72.5	13.79	24.14	38.33	2
40.5	9.74	21.78	32.39	2	73	5.18	14.29	19.03	2
40.5	11.23	25.85	45.44	2	73.5	1.79	9.58	13.29	2
41	11.78	27.62	52.05	2	74.5	9.61	19.49	28.71	2
41.5	14.26	30.69	53.69	2	75	7.44	18.12	34.37	2
42	13.31	31.06	58.07	2	75.5	7.09	18.36	34.38	2
43	14.09	31.68	55.89	2	76	26.96	46.23	65.51	2
43.5	17.15	36.44	63.4	2	76.5	5.99	16.9	32.12	2
44	12.09	26.78	44.23	2	77	10.94	20.27	33.03	2
44.5	8.12	22.26	39.19	2	77.5	34.28	42.05	43.77	74
45	11.21	25.49	37.25	2	78	22.14	30.73	38.9	2
45.5	7.27	20.81	35.41	2	79	13.97	23.52	32.47	2
46	18.81	35.86	59.56	2	79.5	3.81	12.23	23.28	2
46.5	19.39	38.37	62.21	2	80	11.9	19.98	30.32	2
47	22.23	40.9	62.77	2	80.5	3.02	12.43	16	2
47.5	28.32	49.3	70.12	57	81	9.43	21.65	32.62	2
48	23.81	42.12	60.09	50	81.5	9.83	26.32	59.63	2
48.5	32.31	52.22	68.5	66	82	9.89	21.42	34.72	2
49	13.89	27.22	41.94	2	82.5	12.34	21.58	30.38	2
49.5	18.32	40.45	73.07	2	83	16.91	29.47	52.23	2
50	12.06	26.61	47.79	2	83.5	40.46	67.46	80.66	88
50.5	12.36	27.33	50.67	2	84	39.83	69.14	84.91	85
51	11.72	26.03	49.91	2	84.5	38.39	66.56	83.39	81
51.5	7.81	21.54	40.14	2	85	41.69	71.92	85.26	89
51.84	3.69	12.91	25.82	2	85.5	39.83	72.97	90.68	2
52	7.72	20.17	41.88	2	86	32.67	56.04	75.56	2
52.5	6.03	17.57	35.3	2	86.5	37.54	71.34	92.91	2
52.9	6	16.05	32.69	2	87	31.98	50.97	64.97	67
52.9	4.21	13.57	25.22	2	87.5	20.4	33.48	41.67	49
53	5.95	17.43	37.84	2	88	39.66	66.24	80.6	86
53.5	3.9	14.32	32.94	2	88.5	40.31	63.71	74.54	102
53.79	10.31	24.2	44.31	2	89	29.89	51.54	72.26	2
53.79	10.27	23.65	40.67	2	89.5	38.08	59.37	70.84	91
54	11.81	27.17	48.44	2	90	36.46	60.55	76.59	79
54.5	13.57	28.5	46.22	2	90.5	18.93	31	36.91	50
55	12.66	28.3	49.14	2	91	39.23	62.63	76.04	77
55.5	15.42	40.44	81.74	2	91.5	36.4	57.84	71.68	99
55.82	17.82	37.4	59.69	42	92	28.83	45.77	57.71	106
56	6.28	18.97	36.86	2	92.5	14.32	29.21	51.67	2
56.5	7.1	20.38	41.09	2	93	31.08	50.49	66.52	64
57	5.02	16.95	32.53	2	93.5	34.34	53.16	66.67	86
57.5	5.85	17.27	31.58	2	94	52.31	104.17	116.44	111
58	11.5	27.8	53.79	2	95.5	22.32	41.62	61.42	45
58.5	6.96	18.77	36.28	2	96	17.15	33.37	54.53	2
59	7.25	20.36	40.1	2	96.5	48.5	119.91	146.63	299
59.5	9.49	21.86	37.51	2	97	13.8	32.48	64.16	2
60	5.63	16.92	33.13	2	98	34.24	59.33	79.23	64
60.5	8.17	21.71	43.99	2	98.5	15.76	35.76	68.03	2
61	9.74	22.62	35.43	2	101	7.26	22.33	60.36	2
61.5	8.54	20.62	33.56	2	101.5	2.15	11.15	17.56	2
62	8.91	21.62	34.17	2	102	14.47	37.51	76.01	2
62.5	8.21	20.19	32.84	2	102.5	22.67	51.31	84.56	2
63.5	7.5	19.46	36.26	2	103	25.66	57.75	91.1	2
64	8.69	20.6	34.17	2	103.5	23.45	51.91	85.53	2
64.5	8.43	20.42	35.29	2	104	17.9	38.81	69.04	2
65.5	7.5	18.98	32.75	2	104.5	20.13	56.28	101.48	2
66	6.94	19.37	34.06	2	105	19.61	49.29	88.05	2
66.5	5.26	16.12	29.75	2	105.5	15.22	38.34	73.72	2
67	64.42	170.88	137.61	272	106	8.95	25.97	56.75	2
67.5	7.6	18.55	33.04	2	106.5	14.81	33.48	62.97	2
68	7.6	19.06	33.73	2	107	20.83	48.51	84.48	2

Appendix 2 - Continued

Depth (mbsf) Top interval	%Sand (>56um)	Mean	Standard deviation	Mode	Depth (mbsf) Top interval	%Sand (>56um)	Mean	Standard deviation	Mode
107.5	11.25	23.09	38.53	2	143.5	11.32	27.9	62.03	2
108	14.91	34.53	67.52	2	144	9.59	22.69	47.38	2
108.5	23.54	45.41	71.36	2	144.5	6.49	16.53	30.26	2
109	24.22	45.16	66.75	47	145	57.35	145.18	152.33	285
109.5	0.22	6.84	8.29	2	145.5	66.62	181.74	164.32	311
110	10.27	26.54	51.57	2	146	61.19	168.95	166.88	333
110.5	19.86	47.37	81.56	2	146.5	56.68	140.99	148.75	290
111	10.08	26.1	50.72	2	148.5	74.34	202.67	156.26	306
111.5	21.99	43.47	68.66	2	149	66.09	187.34	167.01	341
112	19.48	40.26	67.04	2	150	74.22	216.93	167.85	349
112.5	12.59	31.86	60.84	2	150.5	69.04	210.12	172.99	353
113	34.35	47.84	37.83	55	151	73.3	185.71	149.65	288
113.5	16.56	32.71	54.63	2	151.5	63.45	174.42	161.93	321
114	21.28	37.81	58.45	2	152	61.77	159.81	155.85	311
114.5	7.34	23.52	51.42	2	152.5	57.25	146.28	155.95	281
115	15.22	34.3	63.61	2	153	87.91	190.97	107.87	234
115.5	28.26	56.27	84.5	2	153.5	89.46	203.33	121.22	259
116	27.16	49.92	73.39	2	154	80.07	172.84	126.83	257
116.5	23.12	37.86	52.94	2	154.5	86.65	156.44	94.67	172
117	24.86	41.51	53.73	52	155	86.87	142.68	83.43	146
117.5	34.78	52.49	63.61	68	155.5	78.92	136.04	95.24	163
119	25.36	40.14	47	53	156	70.45	87.02	60.57	99
119.5	21.79	40.06	57.38	46	156.5	67.73	72.57	43.22	82
120	18.5	38.04	60.14	42	157.5	30.21	67.61	101.76	2
120.5	14.62	32.24	54.84	2	158	17.59	37.34	66.92	2
121	13.25	28.4	46.68	2	158.5	29.08	62.87	95.35	2
121.5	15.96	33.67	56	2	159	31.67	64.33	93.4	2
122	13.04	29.3	52.8	2	159.5	7.65	22.74	54.01	2
122.5	18.7	37.16	64.47	2	160	21.59	45.69	74.67	2
123	12.59	28.15	47.71	2	160.5	10.29	27.64	59.63	2
123.5	8.69	25.35	58.51	2	161	11.65	27.77	55.14	2
124	12.4	32.79	63.77	2	161.5	9.81	83.92	184.77	7
124.5	7	20.86	36.42	2	162	14.42	31.35	53.22	2
125	12.34	29.3	52.36	2	162.5	15.64	32.19	56.92	2
125.5	14.14	32.75	61.74	2	163.5	18.27	36.91	64.8	2
126	11.98	31.03	65.98	2	164	16.01	34.32	64.98	2
126.5	12.07	31.4	66.22	2	164.5	15	31.32	60.28	2
127	17.06	39.75	72.53	2	165	14.64	30.36	56.69	2
127.5	12.84	32.79	68.52	2	165.5	15.77	34.05	63.28	2
128	12.62	31.47	64.83	2	166	16.59	33.93	61.37	2
128.5	16.16	38.75	75.76	2	166.5	18.69	38.7	67.72	2
129	21.25	46.38	80.04	2	167	13.85	25.68	38.56	2
129.5	31.75	64.18	91.24	2	167.5	13.16	30.5	63.29	2
130	23.47	44.93	72.02	2	168	15.73	31.07	55.37	2
130.5	10.14	23.22	46.66	2	168.5	16	29.86	50.81	2
131	24.64	47.45	74.53	2	169	27.46	60.36	95.54	2
131.5	25.07	48.16	76.29	2	169.5	37.23	83.79	112.99	349
132	17.95	35.67	63.33	2	170	36.61	79.92	108.08	344
132.5	15.26	31.92	59	2	170.5	39.6	86.72	110.95	341
133	13.99	30.23	58.91	2	171.5	34.94	76.13	105.62	346
133.5	17.45	33.62	56.94	2	172	38.31	82.51	108.13	342
134	12.17	24.68	44.17	2	172.5	36.01	76.49	105.25	346
135	9.39	23.73	51.6	2	173	49.49	128.07	152.17	306
135.5	9.01	21.5	43.3	2	173.5	38.62	84.67	112.01	345
136	12.6	24.91	42.26	2	174	42.26	99.03	123.09	349
136.5	16.09	32.52	58.77	2	174.5	49.74	123.46	138.09	351
137	14.57	28.99	50.17	2	175	9	26.2	54.13	2
137.5	9.45	22.49	48.25	2	175.5	43.14	100.79	123.74	349
138	6.85	16.87	32.75	2	176	51.81	121.79	128.81	349
138.5	11.05	27.73	58.65	2	176.5	80.72	231.27	144.68	291
139	10.21	25.64	54.51	2	177	78.21	225.03	159.96	323
139.5	14.9	32.95	65.59	2	177.5	33.64	46.82	33.96	54
140	15.16	33.1	65.45	2	178	14.13	27.02	40.74	2
140.5	4.82	15.47	33.05	2	179	16.96	33.1	38.11	43
141	8.39	25.31	61.71	2	179.5	40.22	63.29	67.55	56
141.5	4.02	15.44	38.57	2	180	17.28	33.57	50.91	2
142	7.25	20.31	50.22	2	180.5	30.75	46.62	46.69	51
142.5	13.33	32.94	71.14	2	181.5	22.92	40.87	54.66	44
143	8.22	21.23	50.81	2	182	77.55	183.09	140.65	241

Appendix 2 - Continued

Depth (mbsf) Top interval	%Sand (>56um)	Mean	Standard deviation	Mode	Depth (mbsf) Top interval	%Sand (>56um)	Mean	Standard deviation	Mode
182.5	60.51	163.68	161.42	275	204	75.73	240.04	175.49	351
183	76.77	202.65	159.4	260	204.5	59.09	183.51	182.34	414
183.5	59.55	130.41	127.11	237	205	67.63	122.3	101.77	167
184	74.1	174	140.69	233	205.5	24.84	45.55	65.3	49
185	24.24	56.85	97.95	2	206	71.93	114.58	84.53	145
185.5	16.72	35.94	66.94	2	206.5	79.23	159.5	105.64	198
186	26.67	53.37	83.92	2	207	65.24	133.98	107.92	199
186.5	19.42	36.95	61.82	2	207.5	58.83	74.38	61.24	96
187	27.2	59.39	96.32	2	208	84.72	121.13	69.6	128
187.5	9.4	23.52	54.4	2	208.5	79.14	134.4	87.63	161
188	25.51	48.12	75.54	2	209	77.57	143.77	101.3	169
188.5	26.88	42.8	62.88	2	209.5	74.09	132.52	97.49	163
189	2.61	11.57	22.76	2	210.5	41.58	55.36	52.39	63
189.5	24.73	39.42	59.75	2	211	48.74	59.5	47.16	68
190	35.67	72.37	102	2	211.5	41.52	89.42	114.32	298
190.5	42.66	70.88	85.4	95	212	22.38	45.5	70.12	41
191	30.17	52.53	75.39	2	212.5	46.34	74.44	78.15	70
191.5	28.14	60.88	93.55	2	213	19.85	41.77	60.19	31
192	27.11	57.95	88.7	2	213.5	23.08	40.05	49.27	44
192.5	30.54	65.88	96.81	2	214	47.81	63.8	58.27	76
193	17.25	38.84	69.13	2	214.5	20.22	39.28	53.01	34
193.5	15.06	29.69	57.07	2	215	58.63	82.19	68.96	80
194	16.36	31.21	58.42	2	215.5	63.3	98.57	88.85	100
194.5	13.32	29.06	57.88	2	216.5	49.71	86.75	94.47	68
195	10.9	21.72	40.96	2	217.5	55.58	79.26	74.03	81
195.5	23.91	39.26	59.04	2	218	85.62	258.06	163.43	350
196	21.12	43.53	74.05	2	218.5	78.31	255.25	186.14	2
196.5	30.74	51.29	70.12	2	219	74.38	188.63	156.23	293
197	32.63	69.31	99.61	2	219.5	73.89	233.86	178.13	367
197.5	54.39	126.08	143.85	256	220	82.43	263.31	159.18	333
198	27.11	55.12	86.12	2	220.5	81.61	187.92	133.8	248
198.5	29	60.49	91.58	2	221	85.52	192.46	114.85	245
199	30.14	64.6	96.66	2	222	55.92	147.91	155.86	291
199.5	26.26	55.47	88.17	2	224	14.93	35.53	76.09	2
200	51.43	107.55	116.3	344	224.5	15.01	35.05	72.09	2
200.5	46.84	105	123.91	351	225	5.23	17.47	43.09	2
201	39.61	72.45	88.99	69	226.5	79.58	231.72	140.54	290
201.5	41.87	77.12	94.01	2	227	72.65	216.31	151.81	305
202	40.41	89.46	113.11	334	228	66.41	255.4	202.52	2
202.5	52.77	117.98	129.98	254	229	46.8	66.79	69.64	94
203	59.42	148.48	142.16	268	229.5	16.11	26.29	45.03	2
203.5	70.09	129.25	91.39	196	230	56.13	69.68	59.29	94